

MESH - Understanding Videos Like Human: Measuring Hallucinations in Large Video Models

Garry Yang*

The Chinese University of Hong Kong
Hong Kong, Hong Kong SAR
hcyang@cse.cuhk.edu.hk

Zizhe Chen*

The Chinese University of Hong Kong
Hong Kong, Hong Kong SAR
zzchen2@cse.cuhk.edu.hk

Man Hon Wong

The Chinese University of Hong Kong
Hong Kong, Hong Kong SAR
mhwharry@gmail.com

Haoyu Lei

The Chinese University of Hong Kong
Hong Kong, Hong Kong SAR
hylei22@cse.cuhk.edu.hk

Yongqiang Chen

The Chinese University of Hong Kong
Hong Kong, Hong Kong SAR
yqchen@cse.cuhk.edu.hk

Zhenguo Li

Huawei Noah's Ark Lab
Hong Kong, Hong Kong SAR
zhenguo1@gmail.com

Kaiwen Zhou

Huawei Noah's Ark Lab
Shenzhen, China
zhoukaiwen2@huawei.com

James Cheng

The Chinese University of Hong Kong
Hong Kong, Hong Kong SAR
jcheng@cse.cuhk.edu.hk

Abstract

Large Video Models (LVMs) build on the semantic capabilities of Large Language Models (LLMs) and vision modules by integrating temporal information to better understand dynamic video content. Despite their progress, LVMs are prone to hallucinations—producing inaccurate or irrelevant descriptions. Current benchmarks for video hallucination depend heavily on manual categorization of video content, neglecting the perception-based processes through which humans naturally interpret videos. We introduce **MESH**, a benchmark designed to evaluate hallucinations in LVMs systematically. MESH uses a Question-Answering framework with binary and multi-choice formats incorporating target and trap instances. It follows a bottom-up approach, evaluating basic objects, coarse-to-fine subject features, and subject-action pairs, aligning with human video understanding. We demonstrate that MESH offers an effective and comprehensive approach for identifying hallucinations in videos. Our evaluations show that while LVMs excel at recognizing basic objects and features, their susceptibility to hallucinations increases markedly when handling fine details or aligning multiple actions involving various subjects in longer videos.

Keywords

Large Video Models, Video Hallucination, Video Question-Answering

1 Introduction

Large language models (LLMs) [57] excel in handling real-world tasks by responding to user queries and generalizing across multi-modal information, including images, videos, and audio [82]. Open-source models like LLaMA [75] can be pre-trained on modality-specific datasets to align these modalities with language tokens [26], while closed-source models like GPT-4 [60] refine and summarize information from modality-specific encoders [45]. For vision-language tasks, pre-trained vision encoders such as CLIP [62] convert visual inputs into dense visual tokens that capture semantic and spatial layout. A language model encodes the text prompt into

textual tokens. These visual and textual tokens are then aligned and fused to enable joint reasoning across modalities. This integration enables a wide range of downstream tasks, including image captioning, visual question answering (VQA), and image-based storytelling [32, 71]. This architecture, which combines vision and language understanding, constitutes a large vision-language model (LVLM).

Video understanding involves integrating visual, auditory, and temporal cues to interpret dynamic content [72, 74]. Humans naturally track actions, dialogue, and subtle temporal changes across frames. Basic grounding information, such as object locations and identities, serves as the foundation for higher-level comprehension, including emotion recognition [16, 54]. To perform similar tasks, such as video captioning, large vision-language models (LVLMs) first apply sampling techniques to convert videos into sequences of frames, then encode and summarize each frame's visual content to extract semantic meaning and capture temporal dynamics [83]. Through fine-tuning on video datasets, LVLMs can function as large video models (LVMs), enabling more accurate extraction, alignment, and summarization of multimodal information from video content [28].

A key challenge when applying LVMs to video-specific tasks is the exacerbation of hallucination issues [65]. LLMs, which are prone to generating irrelevant or incorrect content in response to prompts [66], face a heightened risk of hallucination due to complex interactions between multiple components [40]. Vision encoders, which are pre-trained to map both visual and textual data into a shared latent space [26, 62], often prioritize correlations learned from training data over accurate visual interpretation [55]. Processing videos generates a large volume of visual tokens from sequential frames, requiring aggressive sampling strategies that risk discarding important information [80]. As illustrated in Figure 1, distinguishing objects or characters and their features requires localizing the relevant frame, while actions spanning multiple frames—such as opening a flag—demand precise summarization of temporally distributed visual tokens [10, 81]. To investigate into the hallucination of video understanding, we pose the following challenge:

*Both authors contributed equally to this research.

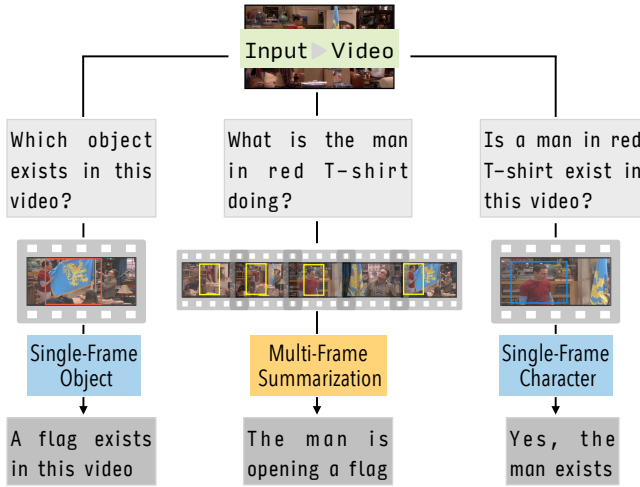


Figure 1: LVMs understand videos.

“Is there a comprehensive benchmark for measuring hallucination in video understanding?”

Most existing benchmarks either adopt caption-based comparisons or adapt the binary question format from POPE [40]. They evaluate LVMs on various aspects, including subject recognition or temporal details [15, 19, 37, 39, 67, 78, 81, 84]. However, most existing approaches depend on manual categorization of video content, leading to questions with varying levels of granularity—for instance, identifying scene transitions (coarse) versus counting specific actions (fine). Currently, there is no perception-based framework for categorizing hallucination types that aligns with how humans intuitively understand video. Humans typically process video in a bottom-up manner: first recognizing the environment and objects (*Setting*), then identifying key individuals (*Character*), and finally interpreting their actions and dialogues (*Stage*) [7, 64]. To replicate this, we target measuring human understanding of the visual aspects of videos and emphasizes *mise-en-scène*, which encompasses all visual elements in videos [7, 24]. *Mise-en-scène* is categorized into three domains: **setting**, **characters**, and **stage**. The **setting** includes the physical environment and objects, providing narrative context and relationships [5, 7]. **Characters** involve physical traits for main subjects, including clothing, contributing to identity portrayal [24]. We focus on distinguishing human characters in this work. **Stage** includes character movements, requiring models to accurately identify action/dialogue sequences and associate them with the relevant subjects [5]. Detailed description is present in Appendix A. To demonstrate the practical use of this perception categorization, we use the TVQA+ dataset [35] for its richer context compared to daily footage. Our method is easily transferable to other datasets, such as UCF101 [69]. The generalized annotation pipeline and experiment results are shown in Appendix B.6. We then create binary and multi-choice questions featuring target and trap instances based on TVQA+ annotations, forming **Mise-En-Scène-Hallucinator (MESH)**. This benchmark assesses LVMs’ capability to recognize basic elements, discern fine details, and detect subject-action pairs in videos with complex interactions.

Using MESH, we conduct extensive experiments across LVMs with various configurations. Our findings are: **1) LVMs struggle**

Table 1: Results with various difficulties of MESH

Model	Advanced	Basic	Average
InternVL2.5-78B	73.4	90.1	85.6
LLaVA-Video-72B	70.1	89.5	84.8
LLaVA-OV-72B	62.4	81.9	77.3
Aria-23B	57.0	81.9	76.6
LLaVA-NV-32B	54.0	76.7	69.6
GPT-4o	58.7	83.8	79.1

with fine character details and aligning multiple actions across subjects in longer videos, despite accurately capturing basic objects and coarse features, as demonstrated by basic and advanced tasks in Table 1. 2) LVMs with weaker performance in Setting/Character aspects **exhibit increased hallucinations when processing spanning frames**, while stronger LVMs maintain accuracy and **leverage multi-frame tokens for finer detail prediction**. 3) MESH results **align with other video understanding benchmarks**, suggesting that mitigating MESH hallucinations improves performance on general tasks.

2 Related Works

2.1 Video Understanding Models

Video understanding tasks [32, 71, 72, 83] traditionally relied on feature extraction techniques to encode relevant video characteristics [8, 20, 27, 53]. The emergence of deep learning techniques has significantly advanced spatial and temporal feature capture [72], outperforming handcrafted methods. To address the lack of task-specific video labels, self-supervised learning [47, 52, 62] enabled the development of general pre-trained video models, finetuned for diverse downstream tasks [83]. Despite advancements, video understanding models still struggle to comprehend the underlying semantic content of each frame and often fail to relate relevant contexts when answering questions involving both visual and chronological data [58, 71]. With the improvement of large language models (LLMs), such as LLaMA [75] and GPT-4 [60], these models have demonstrated a superior ability to understand user queries, including images and videos, and provide detailed answers or explanations without needing further fine-tuning. Techniques like these could facilitate video understanding models to communicate through user prompts, capturing, processing, and summarizing video content to address various tasks [32].

2.2 Measuring Hallucination in Vision Models

In generative models, hallucination refers to outputs deviating from the input source (intrinsic) or established external knowledge (extrinsic) [29, 31]. For LVMs, hallucinations encompass object, multi-modal conflict, counter-knowledge, and attribute types [49, 78, 87]. The POPE framework [40] uses a polling-based question schema to assess object hallucinations with scalability and flexibility, while Liu et al. [48] extend this approach to binary questions for vision and language hallucinations. Video benchmarks challenge LVMs to address hallucinations, such as identifying objects, people, and actions accurately [10, 23, 39, 50, 59, 61]. Many adopt POPE’s question structure to query spatial/temporal contents in videos [4, 15, 19, 37, 39, 78, 81, 84]. For example, Li et al. [39] categorize static/dynamic video content into sub-tasks of varying

granularity, from objects/actions to scenes/states. Cores et al. [19] focus on multi-choice questions with temporally confusing options, while Bansal et al. [4] use contrastive methods to craft convincing negative captions. MESH also generates complex negative options across categories. These benchmarks vary in difficulty due to a lack of bottom-up modeling of human video understanding and often miss key grounding details. A common issue is the neglect of subject-action alignment—humans comprehend videos by recognizing each subject’s specific action. Saravanan et al. [67] constructs negative captioning using entity-action substitution. Compared with Saravanan et al. [67], MESH uses longer videos, richer subject-action pairs, and precise speaker localization.

3 MESH Benchmark

In this section, we provide a comprehensive explanation of our *Mise-En-Scène-Hallucinator* benchmark. This includes both binary and multi-choice (MC) questions that examine various perspectives of a video. Section 3.1 introduces the annotations of the base dataset. Section 3.2 presents the polling pipeline to formulate hallucination questions alongside the evaluation metric. Section 3.3 presents questions concerning hallucinations involving three parts: *Setting with objects*, *Characters with features*, and *Stage with actions/dialogues*.

3.1 Dataset Grounding

We begin by selecting the TVQA+ dataset [35] which provides spatial and temporal annotations along with subtitles as the basis dataset. Figure 2 illustrates the structure of TVQA+, which includes three key components. **Spatial grounding** provides frame-level bounding boxes for objects and characters mentioned in the original questions, such as identifying *flowers*, *bottle*, or characters like *Penny* and *Leonard*. We replace character names by their features, detailed in Appendix B.3.2. **Subtitle** annotates the start and end frames for character dialogues, marking speech timings precisely—for instance, the conversation between *Penny* and *Leonard*. We link speakers’ name with their features, detailed in Appendix B.4.3. **Action timestamp annotation** marks the start and end frames of actions from the original questions, such as identifying actions like “Raj walks into the room”. We align subjects with their features to construct subject-action pairs, detailed in Appendix B.4.4.

3.2 Polling-based Methodology

Empirical results in image hallucination measurements reveal that caption-based benchmarks are unstable, biased towards short captions, and reliant on manual, dataset-specific parsing rules, leading to frequent omissions and misclassifications [40]. To refine hallucination measurement beyond captioning, we extend POPE’s polling-based binary classification method [40] to include MC questions using multiple-probing techniques. This format diversifies negative options, increasing evaluation difficulty and improving LVM performance differentiation [33]. Its effectiveness and robustness are demonstrated in Appendix B.1.1. We illustrate binary and MC question format in Figure 2. **Binary evaluation** involves selecting a ground truth instance (*target*) for positive questions (e.g., *Is a bottle present in this video?*) and a non-existent or fake instance (*trap*) for negative questions (e.g., *Is a bed present in this video?*).

Performance is evaluated using Accuracy, with the Positive Ratio metric accounting for the tendency of LVMs to overproduce “yes” responses. **MC evaluation** constructs MC questions by pairing one *target* with three *trap* instances. Overall accuracy measures the proportion of correct responses, while *Option Balance* (OB) and *Correct Option Balance* (COB) assess the distribution of option selections and correct answers, respectively, using standard deviation formulas, details given in 4.1. The target and trap instances span objects, character features, and actions, depending on the hallucination focus, as discussed further in the next section.

3.3 Benchmark Detail

We present the definition of the question set shared across three dimensions. The target and trap instances in various hallucination aspects are detailed in the following section.

Definition 3.1. We constructs a 3-tuple list for each video clip, consisting of a clip, a *yes-no* question set, and a multi-choice question set. A hallucinator tuple is:

$$\langle v, \{q^b(m_i), a_i^b\}_{i=1}^{l_b}, \{q^c(n_j^+, n_{j_1}^-, \dots, n_{j_k}^-), a_j^c\}_{j=1}^{l_c} \rangle \quad (1)$$

where $\{q^b(m_i), a_i^b\}_{i=1}^{l_b}$ represents the binary question set, with m_i denoting a target (positive m_i^+ , $a_i^b = \text{yes}$) or trap instance (negative m_i^- , $a_i^b = \text{no}$), generated by the template “Is __ present in this video?”. $\{q^c(n_j^+, n_{j_1}^-, \dots, n_{j_k}^-), a_j^c\}_{j=1}^{l_c}$ represents the multi-choice question set, where n_j^+ is a positive instance, $n_{j_1}^-, \dots, n_{j_k}^-$ are k negative instances, and a_j^c is the answer. Questions are generated using the template “Which of the following is *present/speaking/action* in this video?” with $k = 3$ for a four-choice structure.

3.3.1 Setting Hallucination. In this section, we describe how to construct hallucination questions for the **Setting** perspective. The pipeline is outlined in Figure 3. Objects annotations in videos are more sparse, compared with images. We discuss this distinction in Appendix B.2.1. We propose a **space-centered selection method**, where each video clip is assigned a **space label**. For example, in Figure 3, the first video is labeled *restaurant*, while the others are labeled *bedroom* and *bathroom*, respectively. The unique object set for each space label is defined as:

$$O_s \leftarrow \text{Filter} \left(\bigcup_{\{v_y | s_y = s\}} O_y \right) \quad (2)$$

where O_y represents the set of annotated objects in video v_y with label $s_y = s$. *Filter* removes common objects that appear across multiple space labels, ensuring that O_s contains only distinct objects of label s . Detailed steps are provided in Appendix B.2.3. For a video v_x , the targets m_i^+ and n_i^+ in Equation 1 are directly selected from the annotated objects within its frames. Conversely, the traps for are selected from object sets associated with different space labels:

$$m_i^-, n_i^- \leftarrow \text{RandomSelect} \left(\bigcup_{\{s \neq s_x\}} O_s \right). \quad (3)$$

This ensures that trap objects belong to spaces other than v_x , thereby enforcing the space-aware selection criterion.

3.3.2 Character Hallucination. In this section, we present how to construct hallucination questions for the **Characters with their Features**. The detailed pipeline is illustrated in Figure 4. Human characters have been the subjects for most videos, despite their

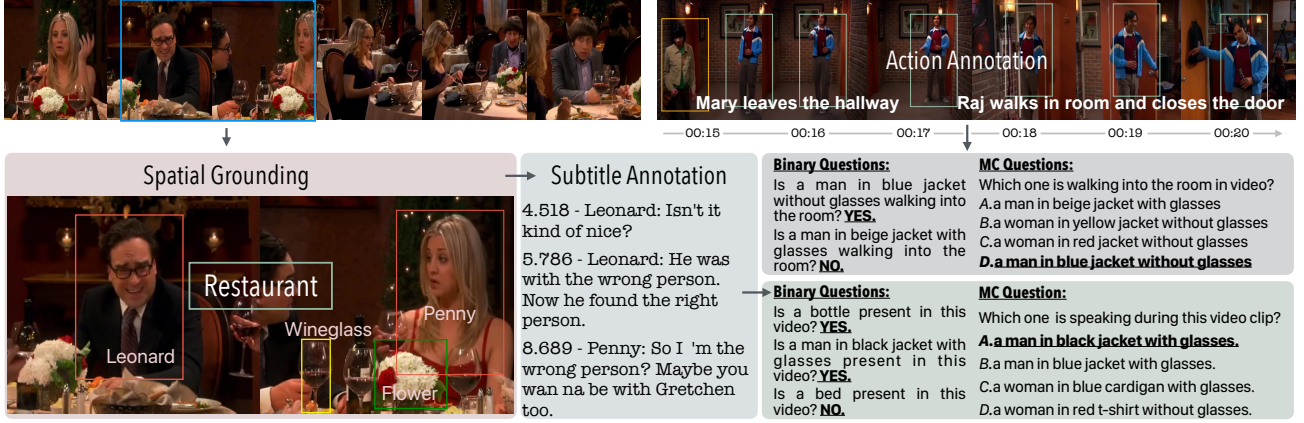


Figure 2: Space Grounding and Subtitle/Action Annotations from TVQA+ and example questions

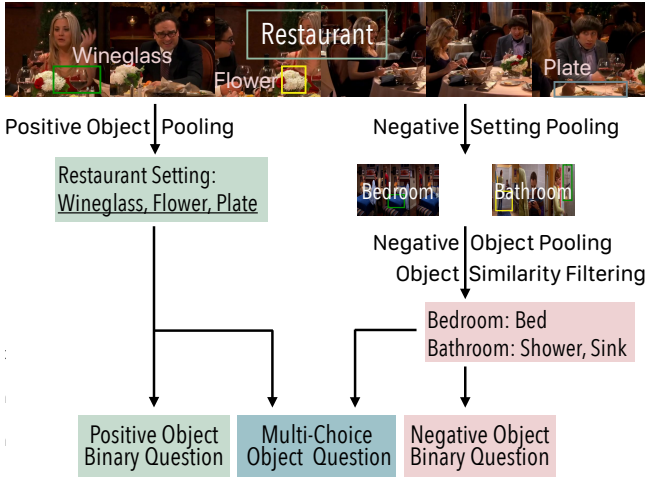


Figure 3: Constructing setting hallucination questions

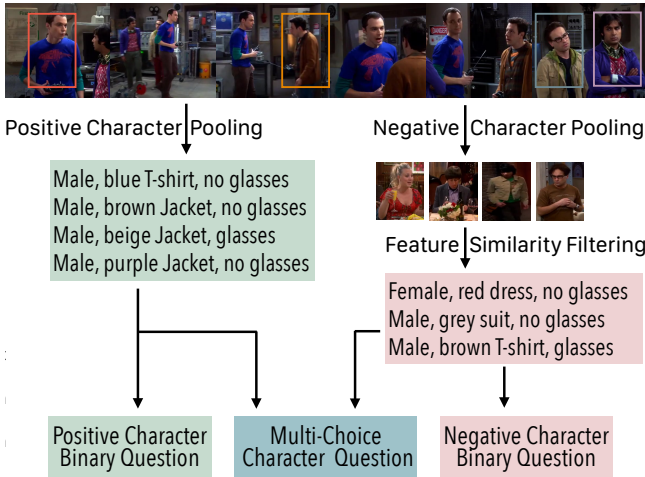


Figure 4: Constructing character hallucination questions

lower average density compared to objects. Therefore, precisely localizing and distinguishing different characters by their features are key to complex video understanding. We demonstrate this in detail in Appendix B.3.1.

Character Features in Videos: In the TVQA+ dataset [35], main characters appear without shielding or background blurring, allowing for clear identification of character features. As shown in Figure 4, videos include multiple characters in various appearances, providing a basis for distinguishing each. For a video v_x , the k -th character is denoted as c_{xk} . We utilize GPT4o [30] to perform initial auto-detection of character features, with manual adjustments for errors. Detailed annotation process is presented in Appendix B.3.2. Features include gender f_{ge} , garment type f_t , garment color f_c , glasses f_{gl} , sleeve type f_{sl} , collar presence f_{co} , pocket presence f_p , and garment shade f_{sh} . Ambiguous cases are labeled as “unknown.” The k -th character in v_x is represented by the feature vector:

$$\mathbf{f}_{xk} = \{f_{ge}(c_{xk}), f_t(c_{xk}), f_c(c_{xk}), f_{gl}(c_{xk}), f_{sl}(c_{xk}), f_{co}(c_{xk}), f_p(c_{xk}), f_{sh}(c_{xk})\}. \quad (4)$$

Selection of Target and Trap Instances: For video v_x , a subset of annotated features is selected to represent different hallucination levels (coarse, medium, fine), forming the target feature set $\{\mathbf{g}_{xk}\}_{k=1}^{l_{xc}}$, where l_{xc} is the number of characters in the video. To construct the trap candidate set \mathcal{G}_{neg} , features are randomly selected from videos other than v_x , and similarity metrics are applied to exclude indistinguishable instances:

$$\mathcal{G}_{neg} = \{\mathbf{g}_{yk} \mid v_y \neq v_x \text{ and } \mathbf{g}_{yk} \neq \mathbf{g}_{xk}, \forall y, k\}. \quad (5)$$

A suitable number of negative instances are then sampled from \mathcal{G}_{neg} for binary and MC questions. Detailed selection algorithms and similarity metrics are provided in Appendix B.3.3.

3.3.3 Stage Hallucination. In this section, we describe the construction of hallucination questions for the **Stage with Actions/Dialogues**. Actions conducted by a given character across multiple frames serve as unique key content in videos. We illustrate its importance in video understanding in detail in Appendix B.4.1. Based on the nature of actions, we divide them into **Dialogue-based** and **Action-based** ones.

Annotating Stage in Videos: For dialogues in Figure 5a, we construct the *subject-within-clip* set using subtitles with their start/end frames, along with character features:

$$\{t_{xk}\}_{k=1}^{l_{xt}} \text{ where } t_{xk} = \langle \mathbf{g}_{xk}^{coarse}, \text{frame}_{sta}, \text{frame}_{end} \rangle. \quad (6)$$

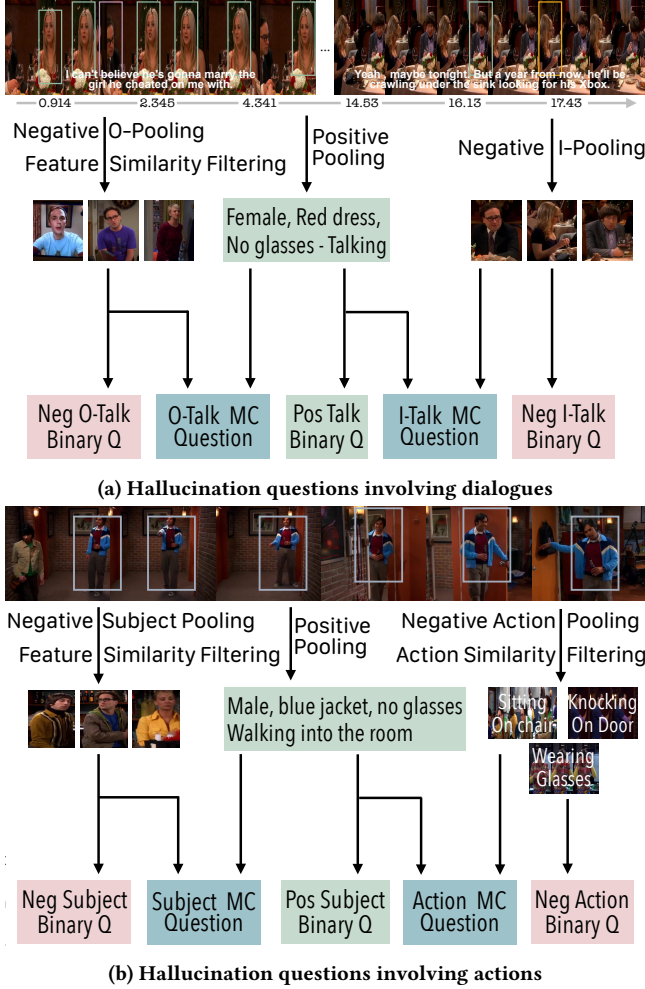


Figure 5: Constructing stage hallucination questions

For actions in Figure 5b, we construct the *subject-action* annotation set:

$$\{a_{xk}\}_{k=1}^{l_{xa}} \text{ where } a_{xk} = \langle g_{xk}^{coarse}, act_{xk} \rangle. \quad (7)$$

l_{xt} and l_{xa} denotes the number of annotated talkings/actions.

Selection of Target and Trap Instances: For video v_x , the target instances are derived from the dialogue-based annotated set $\{t_{xk}\}_{k=1}^{l_{xt}}$ (ET) and the action-based annotated set $\{a_{xk}\}_{k=1}^{l_{xa}}$ (EA). For each target instance, we select dissimilar character features $g_{xk}^{coarse-}$ either from the negative candidate set \mathcal{G}_{neg} (Eq. 5) (CO) or the other characters within the video (CI) and substitute g_{xk}^{coarse} with it to form a trap instance

$$t_{xk}^- = \langle g_{xk}^{coarse-}, frame_{sta}, frame_{end} \rangle \quad (8)$$

for dialogue and for action pairs

$$a_{xk}^- = \langle g_{xk}^{coarse-}, action_{xk} \rangle. \quad (9)$$

We also apply a substitution technique for action pairs. First, we construct the negative action candidate set:

$$\mathcal{A}_{neg} = \{act_{yk} \mid v_y \neq v_x \ \& \ act_{yk} \neq act_{xk}, \forall y, k\}. \quad (10)$$

Then, we either randomly select negative actions act_{xk}^- from \mathcal{A}_{neg} (AO) or generate similar actions (SA) to substitute act_{ik} , forming a trap instance: $a_{xk}^- = \langle f_{xk}, act_{xk}^- \rangle$. Besides, we also mix subject-action pairs by swapping their roles within the video (MI). The detailed selection algorithm and similarity metrics are provided in Appendix B.4.5.

4 Experiments with MESH

We evaluate selected LVMs using MESH. For each video, we generate binary classification and multi-choice (MC) questions targeting setting, character, and stage perspectives to assess hallucination levels. Detailed dataset statistics, LVM characteristics, and experimental technical details are provided in Appendix C.1. In Section 4.2, we present and analyze the results. Through ablation studies in Section 4.3, we verify that MESH distinguishes LVMs based on multi-frame understanding abilities and examines the impact of hallucination levels on Video Question Answering (VQA) benchmarks.

4.1 Experiments Details

Question format. We use both binary and multi-choice (MC) formats. Binary question sets balance positive and negative instances, while MC questions pair one ground-truth with three negatives to assess multiple video contents efficiently, reducing LVM inference costs. MC also enhances clarity by reducing ambiguity in nuanced actions and improves model discrimination by minimizing subjective bias and random variability. Detailed analysis is in Appendix B.1.1.

Table 2: Answer Distribution by Aspect and Category

Aspect	Class	Category Counts			
Setting	Binary	Yes:14663		No:13975	
	MC	A:3646	B:3651	C:3598	D:3713
Character	Binary	Yes:10512		No:10512	
	MC	A:5199	B:5413	C:5197	D:5215
Action	Binary	Yes- EA:2491			
		No- AO:6518 CO:7131 SA:1200 MI:240			
	MC	AO- A:865	B:868	C:896	D:905
		CO- A:1149	B:1177	C:1190	D:1121
		SA- A:880	B:874	C:935	D:908
		MI- A:59	B:73	C:66	D: 82
Dialogue	Binary	Yes- ET: 2303			
		No- AO: 5646 CO: 6756 CI: 1450			
	MC	CO- A: 577	B: 576	C: 569	D: 605
		CI- A: 563	B: 566	C: 588	D: 610

Dataset statistics. **Setting** and **Character** datasets are structured as binary classification and multiple-choice tasks with balanced options. **Stage** datasets contains dialogue/action questions with mixed negative sampling strategies as shown in 3.3.3. Detailed distribution is shown in Table 2

Evaluation metric. We use *accuracy* to measure the proportion of correct answers in both formats. To assess if LVMs are biased toward specific options, we introduce additional balance metrics . For binary questions, the *positive rate* (Pos) reflects the model's

tendency to answer “yes”. In MC questions, *Option Balance (OB)* and *Correct Option Balance (COB)* assess bias across the four choices:

$$OB = \sqrt{\frac{1}{4} \sum_{i=1}^4 (P_i - \bar{P})^2}, \quad COB = \sqrt{\frac{1}{4} \sum_{i=1}^4 (P_i^+ - \bar{P}^+)^2} \quad (11)$$

where $P_i = N_i/N$ and $P_i^+ = N_i^+/N^+$, with N_i and N_i^+ denoting the number of total and correct predictions for option i , respectively. Lower OB and COB values indicate more balanced predictions.

4.2 Experiments Results

Table 3: LVMs’ performances on Setting for Binary/MC tasks.

Model	Binary (%)		MC (%)		
	Acc	Pos	Acc	OB	COB
LLaVA-NV-32B [†]	63.0	86.3	81.4	2.78	1.35
Oryx-7B [‡]	68.4	22.4	62.6	3.26	1.73
VideoXL-7B [‡]	77.1	50.2	73.0	0.93	0.67
Oryx1.5-32B [§]	69.0	23.3	62.8	5.84	2.70
Qwen2VL-72B [‡]	78.4	31.4	86.3	1.52	0.90
VideoLLaMA2.1-7B [‡]	82.6	36.1	84.9	2.51	1.21
LLaVA-OV-72B [‡]	83.8	51.4	83.0	3.13	1.61
LLaVA-Video-72B [‡]	90.3	49.1	92.3	0.76	0.65
InternVL2.5-78B [§]	86.9	40.1	94.9	0.71	0.52
LongVILA-8B [#]	80.7	83.5	76.2	13.7	8.13
VILA1.5-8B [#]	87.2	48.1	66.3	1.58	0.57
LLaMA-VID-LV-7B [★]	47.2	30.8	23.5	36.9	37.3
LLaMA-VID-13B [★]	80.1	65.6	54.2	19.7	9.76
LLaVA-NV-7B [★]	76.1	28.3	81.9	5.77	2.43
Aria-23B [§]	90.0	43.4	85.6	1.95	0.80
VideoAgent [‡]	72.4	51.0	66.4	3.10	2.08
GPT-4o	92.6	50.4	86.6	2.65	2.30

Backbones: [†] Qwen1.5, [‡] Qwen2, [§] Qwen2.5, [#] Llama3, [★] Vicuna, [§] Aria, [‡] Agent.

4.2.1 Setting Hallucination. For each LVM, 32 frames are sampled, centered around the frame where the positive object appears. Table 3 show that LLaVA-Video-72B and InternVL2.5-78B models outperform others in both binary classification and MC tasks. Performance variations among LVMs with different architectures, training strategies, and datasets underscore the influence of these factors on hallucination levels. For example, LLaVA-Video-72B exhibits superior performance compared to LLaVA-OV-72B, primarily due to the inclusion of additional video data during fine-tuning. Conversely, the improved LLM backbone in Oryx1.5-32B does not notably reduce hallucination compared to Oryx-7B, likely due to limitations in the training data or video compression module. In MC tasks, model accuracy generally aligns with binary task performance, except for LLaVA-NV-32B, whose bias toward positive answers amplifies hallucination issues. The OB and COB performances remain low, indicating minimal differences in option selection probabilities and confirming the robustness of our MC format in supplementary to the binary pipeline. In all, our benchmark shows that state-of-art models (e.g., *InternVL2.5*) exhibit reduced hallucination compared to earlier ones (e.g., *Video-LLaVA*), suggesting that improvements in video understanding correlate with less hallucination in setting aspect. These gains stem from architectural changes, including stronger LLM backbones, and the cleaning of training data [11]. Besides, models with high downsampling ratios in their multi-modal adapters (e.g., *LLaMA-VID*) perform worse than those with lower ratios (e.g., *LLaVA-Video-7B*), likely due to loss of fine-grained visual details. Agent-based models like *VideoAgent*, although equipped with strong LLMs, are limited by their external tools (e.g., CLIP

[62]), leading to inferior performance. Surprisingly, scaling LLM parameters shows diminishing returns. In multiple series (*LLaVA-Video*, *LLaVA-OV*, *Qwen2VL*), 7B and 72B models perform similarly, with drastic performance drops only in very small models (e.g., 0.5B). A notable exception is *InternVL2.5-78B*, which achieves best performance using a significantly larger vision encoder, indicating the vision encoder becomes the bottleneck at scale. Long-video fine-tuning (e.g., *LLaMA-VID-7B-Long-Video*) leads to degraded performance, suggesting it may hurt object-level perception. Models with sharing architecture and training data (e.g., *LLaVA-Video* and *LLaVA-OV*) witness significant performance difference due to video-specific finetuning, showing our benchmark captures video-specific hallucination challenges beyond image-based evaluation. The supplementary experiment details and results are in Appendix C.2.

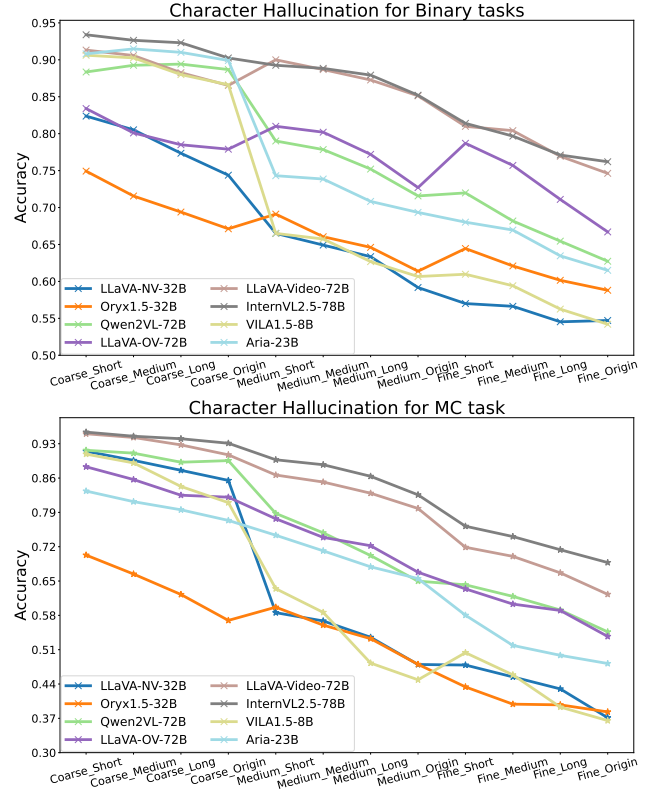


Figure 6: Character Hallucination for Binary/MC tasks.

4.2.2 Character Hallucination. We design experiments at coarse, medium, and fine-grain levels to evaluate hallucination difficulties, ranging from general to detailed character features. We also measure hallucination levels using video clips of varying lengths: *short* (8 frames), *medium* (16 frames), *long* (32 frames), and *origin* (64 frames), centered on the frame with the largest bounding box for the character. Selected results for grain levels and clip lengths are summarized in Figure 6. Overall, performance on *character* aligns with *setting*. LLaVA-Video-72B and InternVL2.5-78B consistently outperform others across grain levels and clip lengths. LVMs show a steeper performance drop in MC tasks than binary tasks, mainly due to challenges in distinguishing multiple characters with fine-grained features across longer videos. Besides, performance declines significantly from coarse to fine-grain levels, demonstrating the

increased difficulty of identifying detailed character features. This challenge stems from: (1) Aggressive token reduction via pooling (e.g., 2×2 or 4×4 layers) [51, 72], which sacrifices detail for efficiency and (2) training data often lacks detailed person descriptions, relying mostly on coarse attributes like gender or clothing color [86]. (3) Fine character features may not be fully captured within a single frame, necessitating LVMs to aggregate features across multiple frames, thereby increasing complexity. Performance also deteriorates with longer clips, as additional frames often introduce noise rather than useful context [41]. Detailed analysis is provided in 4.3.1. In all, LVMs trade off long-context understanding for detail perception when handling fine-grained questions in long videos. Token reduction aids efficiency but reduces granularity, limiting top models like InternVL2.5 to below 0.7 accuracy on the hardest MC setting. Model size has little effect on simple tasks like *Coarse-Short* but greatly impacts advanced tasks like *Fine-Origin*, where larger models significantly outperform smaller ones. This suggests increasing parameter size could effectively capture and retain fine-grained details in complex video scenarios. Additional results and analysis are in Appendix C.3.

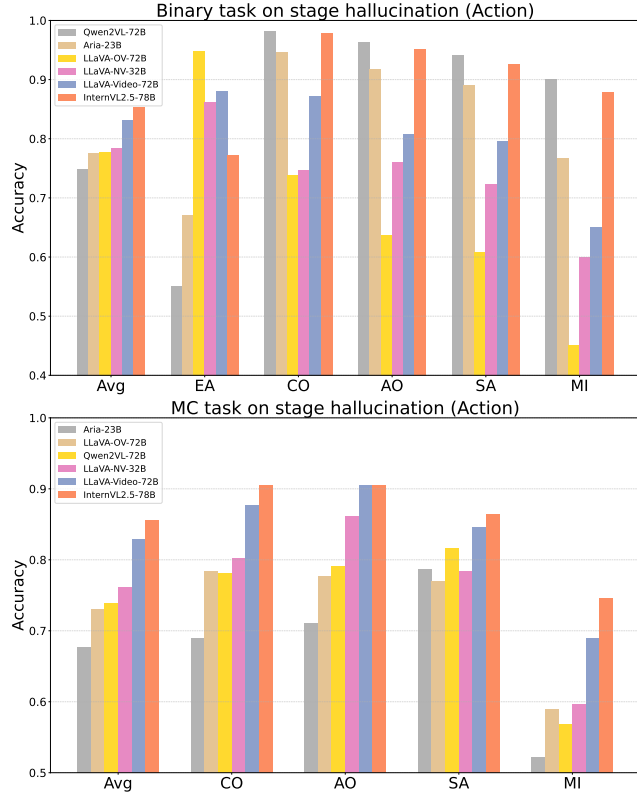


Figure 7: Action Hallucination for Binary/MC tasks

4.2.3 Stage Hallucination. The stage hallucination problems relate subjects with coarse-level character features to their actions. We categorize the questions into *Action* and *Dialogue* types. For **Action** tasks, video annotations for this category follow the format *S* (subject with character features) + *A* (action), e.g., “a man wearing a red jacket (*S*) is walking on the street (*A*).” We identify and merge semantically equivalent actions in AO and CO via vector-based similarity, and use a generation pipeline to produce similar but distinct

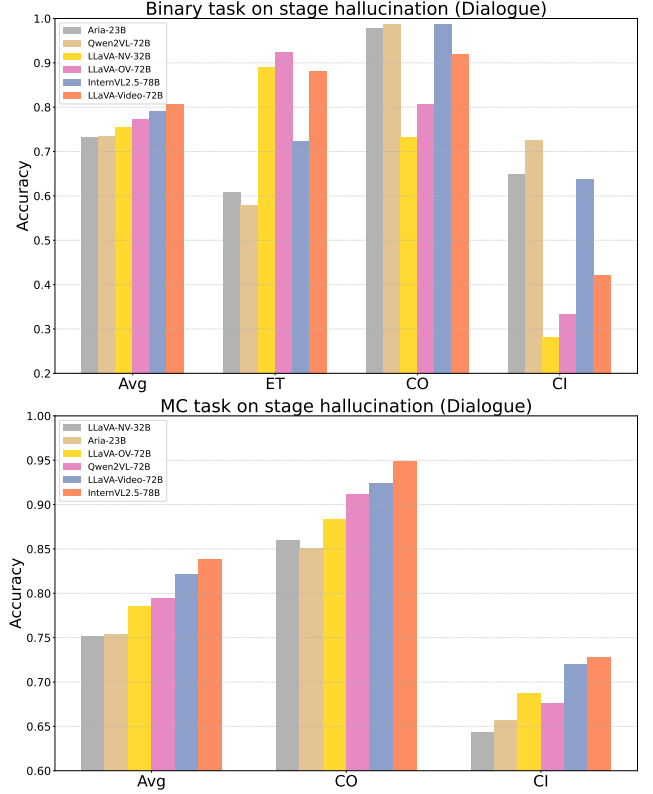


Figure 8: Dialogue Hallucination for Binary/MC tasks

actions for SA. Using positive action annotations, we extract the center action frame and sample 32 frames around it to construct clip instances. Figure 7 shows that average accuracy aligns with previous performance trends. LVMs perform worse on the CO category than on object or character alone, suggesting that combining objects and character into events adds complexity rather than clarity. SA and MI tasks are more challenging than EA, CO, and AO, suggesting that LVMs struggle to differentiate similar actions and align multiple subject-action pairs within the same video. One reason is the high variability of human actions. Unlike static objects with consistent forms, human could move and interact with objects in highly flexible ways. This complexity requires more video-language data for LVMs to learn effectively, but current datasets remain insufficient [86]. Besides, models like InternVL2.5-78B exhibit biases in answering binary questions, performing well on negative questions but showing less confidence in positive EA predictions. For **Dialogue** tasks, annotations for dialogue-based videos follow the format *S* (subject: character features) + “is talking,” e.g., “a man wearing a red jacket (*S*) is talking.” Conversation clips are extracted at 1fps based on subtitle annotations, with variable frame lengths. Figure 8 shows that LVMs perform well on ET and CO tasks in both binary and multiple-choice (MC) formats. However, CI tasks, which require accurately identifying the speaking character within a group, remain significantly more challenging. The sharp drop in CI performance highlights the limitations of current LVMs in recognizing speakers based solely on visual clues. In both stage aspects, models in MC tasks remain stable across sections despite

additional false options, aligning with their average performance and confirming the MC metric’s reliability. By incorporating multiple actions’ timestamps and contexts, we create extended questions that require LVMs to determine whether an action occurs before or after another action. Results are given in Appendix B.5. This allows us to further evaluate the models’ hallucinate on stage and their understanding of spatio-temporal relations. Additional results and analysis are in Appendix C.4.

4.3 Ablation study

4.3.1 Hallucination in images vs. videos. We present the comparison with utilizing a single frame containing the related objects/characters/motions to illustrate the uniqueness of MESH categorization.

Table 4: Setting for Image vs. Video

Model	Binary %		MC %	
	Img.	Vid.	Img.	Vid.
LLaVA-Video-7B	83.7	↑90.6	92.7	↓92.1
Aria-23B	84.2	↑90.0	87.2	↓85.6
InternVL-8B	79.5	↓78.4	90.4	↓82.4
Qwen2VL-7B	88.0	↓85.9	86.2	↓73.2
Oryx-7B	83.6	↓68.4	89.6	↓62.6
LLaVA-NV-32B	85.7	↓63.0	85.6	↓81.4

Setting: longer videos distract LVMs. For setting aspect, the image frame is sampled where the target object occupies its largest area. The result is in Table 4. In the binary task, LVMs with strong performance exhibit increased accuracy when prompted with more frames (Vid.), demonstrating their ability to leverage multi-frame information to reduce hallucination. Conversely, LVMs with poor performance experience a significant drop in accuracy, with declines reaching up to 20%. In the MC task, all LVMs show a performance decrease, with the largest drops observed in underperforming models. This further confirms that our MC structure provides a more challenging and effective metric for measuring hallucination in localizing relevant frames.

Table 5: Character in Continu/Discrete frames (Binary)

Model	Continuous %		Discrete %	
	1 Fra.	4 Fra.	1 Fra.	4 Fra.
LLaVA-Video-7B	77.8	↑78.8	77.8	↓70.7
Aria-23B	64.6	↑69.7	64.6	↓62.6
InternVL-8B	67.0	↓62.9	67.0	↓59.6
Qwen2VL-7B	82.3	↓76.3	82.3	↓67.7
Oryx-7B	68.7	↓59.6	59.0	↓46.6
LLaVA-NV-32B	68.2	↓61.6	68.2	↓61.1

Character: frame continuity matters. For the character aspect, we use fine-grained features to evaluate LVMs’ ability to associate relevant frames for prediction. The result is in Table 5. Continuous frames are sampled around the center frame, while discrete frames are uniformly sampled across the video. With more frames, LLaVA-Video and Aria demonstrate higher accuracy, leveraging multi-frame tokens to better identify characters, while other LVMs are distracted by spanning frames. In contrast, with discrete

sampling, all LVMs show reduced accuracy, suggesting irrelevant frames introduce noise when propagated through frame tokens.

Table 6: Stage (Action) for Image vs. Video

Model	Binary %		MC %	
	1 Fra.	32 Fra.	1 Fra.	32 Fra.
LLaVA-Video-7B	70.5	↑80.9	60.1	↑82.3
Aria-23B	68.5	↑77.5	67.1	↑67.7
InternVL-8B	67.9	↑71.0	56.7	↑76.6
Qwen2VL-7B	72.8	↑78.3	57.1	↑67.2
Oryx-7B	68.7	↓59.6	59.0	↓46.6
LLaVA-NV-32B	68.2	↑78.4	59.3	↑76.1

Stage: seeing actions needs multiple frames. For stage aspect, we compare results between prompting a single action-centered frame and 32 frames. Understanding actions requires LVMs to integrate tokens across multiple frames. Table 6 shows that a single frame is insufficient for accurate judgment, highlighting MESH’s uniqueness in video understanding. Furthermore, high-performing LVMs achieve significant gains with longer video prompts, while low-performing LVMs show limited improvement. This demonstrates that our stage hallucination question set effectively distinguishes LVMs based on their ability to capture chronological action information across the entire video.

Table 7: LVMs’ on MESH vs. VQA tasks

Model	MESH %		VQA %	
	Base	Adv	VMME	MLVU
InternVL2.5-78B	90.1	73.4	72.1	75.7
LLaVA-Video-72B	89.5	70.1	70.6	74.4
LLaVA-OV-72B	81.9	62.4	66.3	68.0
Aria-23B	81.9	57.0	67.6	70.6
LLaVA-NV-32B	76.7	54.0	60.2	65.5
GPT-4o	83.8	58.7	71.9	64.6

4.3.2 Hallucination level aligns with VQA. We calculate base and advanced hallucination levels based on question difficulties (see Appendix C.1.1). Table 7 shows that hallucination levels measured by MESH align with VQA benchmarks (V-MME [23] and MLVU [88]), despite their distinct focus. LVMs with advanced video element detection, from basic to fine details, are better at answering complex questions accurately. However, most LVMs struggle more with advanced hallucination tasks than with VQA tasks. This indicates that fine-grained hallucination questions remain underutilized in VQA. We also show in Appendix E that when LVMs hallucinate on MESH questions, they often produce incorrect or ambiguous video descriptions. Incorporating finer hallucination aspects could enhance high-level VQA task design.

5 Conclusion

In this work, we introduce a bottom-up approach, inspired by human video cognition, to assess LVM hallucinations across setting, character, and stage perspectives (*Mise-En-Scène*). We enhance evaluation with binary and multi-choice questions. Using this framework, we created MESH, a comprehensive benchmark building upon TV series with complex human activities spanning basic to

advanced difficulty levels. Extensive experiments on diverse LVMS configurations revealed that while these models excel at recognizing basic elements from a single frame, their susceptibility to hallucinations increases significantly when handling fine character details or associating multiple actions across frames. We also demonstrate MESH effectively differentiates LVMS capable of leveraging multi-frame tokens to detect fine features and actions, with stronger models performing better in VQA and captioning tasks. These findings confirm the effectiveness and stability of our evaluation pipeline and benchmark.

References

- [1] Aakanksha and A. N. Rajagopalan. 2023. Improving Robustness of Semantic Segmentation to Motion-Blur Using Class-Centric Augmentation. In *IEEE/CVF Conference on Computer Vision and Pattern Recognition, CVPR 2023, Vancouver, BC, Canada, June 17-24, 2023*. IEEE, 10470–10479. doi:10.1109/CVPR52729.2023.01009
- [2] Anthropic. 2024. Introducing Claude 3.5 Sonnet. <https://www.anthropic.com/news/claude-3-5-sonnet>
- [3] Jinze Bai, Shuai Bai, Yunfei Chu, Zeyu Cui, Kai Dang, Xiaodong Deng, Yang Fan, Wenbin Ge, Yu Han, Fei Huang, Binyuan Hui, Luo Ji, Mei Li, Junyang Lin, Runji Lin, Dayiheng Liu, Gao Liu, Chengqiang Lu, Keming Lu, Jianxin Ma, Rui Men, Xingzhang Ren, Xuancheng Ren, Chuanqi Tan, Sinan Tan, Jianhong Tu, Peng Wang, Shijie Wang, Wei Wang, Shengguang Wu, Benfeng Xu, Jin Xu, An Yang, Hao Yang, Jian Yang, Shusheng Yang, Yang Yao, Bowen Yu, Hongyi Yuan, Zheng Yuan, Jianwei Zhang, Xingxuan Zhang, Yichang Zhang, Zhenru Zhang, Chang Zhou, Jingren Zhou, Xiaohuan Zhou, and Tianhang Zhu. 2023. Qwen Technical Report. *CoRR* abs/2309.16609 (2023). arXiv:2309.16609 doi:10.48550/ARXIV.2309.16609
- [4] Hritik Bansal, Yonatan Bitton, Idan Szepes, Kai-Wei Chang, and Aditya Grover. 2024. VideoCon: Robust Video-Language Alignment via Contrast Captions. In *IEEE/CVF Conference on Computer Vision and Pattern Recognition, CVPR 2024, Seattle, WA, USA, June 16-22, 2024*. IEEE, 13927–13937. doi:10.1109/CVPR52733.2024.01321
- [5] Bruce Block. 2020. *The visual story: Creating the visual structure of film, TV, and digital media*. Routledge.
- [6] David Bordwell. 2005. *Figures traced in light: On cinematic staging*. Univ of California Press.
- [7] D. Bordwell and K. Thompson. 2008. *Film Art: An Introduction*. McGraw Hill. <https://books.google.com.hk/books?id=g6ZAAQAIAAJ>
- [8] Paulo Vinicius Koerich Borges, Nicola Conci, and Andrea Cavallaro. 2013. Video-based human behavior understanding: A survey. *IEEE transactions on circuits and systems for video technology* 23, 11 (2013), 1993–2008.
- [9] Zheng Cai, Maosong Cao, Haojiang Chen, Kai Chen, Keyu Chen, Xin Chen, Xun Chen, Zehui Chen, Zhi Chen, Pei Chu, Xiaoyi Dong, Haodong Duan, Qi Fan, Zhaoye Fei, Yang Gao, Jiaye Ge, Chenya Gu, Yuzhe Gu, Tao Gui, Aijia Guo, Qipeng Guo, Conghui He, Yingfan Hu, Ting Huang, Tao Jiang, Penglong Jiao, Zhenjiang Jin, Zhikai Lei, Jiaxing Li, Jingwen Li, Linyang Li, Shuaibin Li, Wei Li, Yining Li, Hongwei Liu, Jiangning Liu, Jiawei Hong, Kaiwen Liu, Kuikun Liu, Xiaoran Liu, Chengqi Lv, Haijun Lv, Kai Lv, Li Ma, Runyuan Ma, Zerun Ma, Wenchang Ning, Linke Ouyang, Jiantao Qiu, Yuan Qu, Fukai Shang, Yunfan Shao, Demin Song, Zifan Song, Zhihao Sui, Peng Sun, Yu Sun, Huanze Tang, Bin Wang, Guoteng Wang, Jiaqi Wang, Jiayu Wang, Rui Wang, Yudong Wang, Ziyi Wang, Xingjian Wei, Qizhen Weng, Fan Wu, Yingting Xiong, Chao Xu, Ruiliang Xu, Hang Yan, Yirong Yan, Xiaogui Yang, Haochen Ye, Huaiyuan Ying, Jia Yu, Jing Yu, Yuhang Zang, Chuyu Zhang, Li Zhang, Pan Zhang, Peng Zhang, Ruijie Zhang, Shuo Zhang, Songyang Zhang, Wenjian Zhang, Wenwei Zhang, Xingcheng Zhang, Xinyue Zhang, Hui Zhao, Qian Zhao, Xiaomeng Zhao, Fengzhe Zhou, Zaida Zhou, Jingming Zhuo, Yicheng Zou, Xipeng Qiu, Yu Qiao, and Dahua Lin. 2024. InternLM2 Technical Report. arXiv:2403.17297 [cs.CL]
- [10] Guangyi Chen, Xiao Liu, Guangrun Wang, Kun Zhang, Philip H. S. Torr, Xiao-Ping Zhang, and Yansong Tang. 2023. Tem-adaptor: Adapting Image-Text Pretraining for Video Question Answer. In *IEEE/CVF International Conference on Computer Vision, ICCV 2023, Paris, France, October 1-6, 2023*. IEEE, 13899–13909. doi:10.1109/ICCV51070.2023.01282
- [11] Zhe Chen, Weiyun Wang, Yue Cao, Yangzhou Liu, Zhangwei Gao, Erfei Cui, Jinguo Zhu, Shenglong Ye, Hao Tian, Zhaoyang Liu, et al. 2024. Expanding Performance Boundaries of Open-Source Multimodal Models with Model, Data, and Test-Time Scaling. *arXiv preprint arXiv:2412.05271* (2024).
- [12] Zhe Chen, Jiannan Wu, Wenhai Wang, Weiye Su, Guo Chen, Sen Xing, Muyan Zhong, Qinglong Zhang, Xizhou Zhu, Lewei Lu, et al. 2024. InternVL: Scaling up vision foundation models and aligning for generic visual-linguistic tasks. In *Proceedings of the IEEE/CVF Conference on Computer Vision and Pattern Recognition*. 24185–24198.
- [13] Zesen Cheng, Sicong Leng, Hang Zhang, Yifei Xin, Xin Li, Guanzheng Chen, Yongxin Zhu, Wenqi Zhang, Ziyang Luo, Deli Zhao, and Lidong Bing. 2024. VideoLLaMA 2: Advancing Spatial-Temporal Modeling and Audio Understanding in Video-LLMs. *arXiv preprint arXiv:2406.07476* (2024). <https://arxiv.org/abs/2406.07476>
- [14] Wei-Lin Chiang, Zhuohan Li, Zi Lin, Ying Sheng, Zhanghao Wu, Hao Zhang, Lianmin Zheng, Siyuan Zhuang, Yonghao Zhuang, Joseph E. Gonzalez, Ion Stoica, and Eric P. Xing. 2023. Vicuna: An Open-Source Chatbot Impressing GPT-4 with 90%* ChatGPT Quality. <https://lmsys.org/blog/2023-03-30-vicuna/>
- [15] Wey Yeh Choong, Yangyang Guo, and Mohan S. Kankanhalli. 2024. VidHal: Benchmarking Temporal Hallucinations in Vision LLMs. *CoRR* abs/2411.16771 (2024). arXiv:2411.16771 doi:10.48550/ARXIV.2411.16771
- [16] Charles Ed Chubb, Barbara A Doshier, Zhong-Lin Ed Lu, and Richard M Shiffrin. 2013. *Human information processing: Vision, memory, and attention*. American Psychological Association.
- [17] Jihoon Chung, Cheng-hsin Wu, Hsuan-ru Yang, Yu-Wing Tai, and Chi-Keung Tang. 2021. HAA500: Human-Centric Atomic Action Dataset with Curated Videos. In *2021 IEEE/CVF International Conference on Computer Vision, ICCV 2021, Montreal, QC, Canada, October 10-17, 2021*. IEEE, 13445–13454. doi:10.1109/ICCV48922.2021.01321
- [18] LMDeploy Contributors. 2023. LMDeploy: A Toolkit for Compressing, Deploying, and Serving LLM. <https://github.com/InternLM/lmdeploy>.
- [19] Daniel Cores, Michael Dorkenwald, Manuel Mucientes, Cees G. M. Snoek, and Yuki M. Asano. 2025. Lost in Time: A New Temporal Benchmark for VideoLLMs. arXiv:2410.07752 [cs.CV] <https://arxiv.org/abs/2410.07752>
- [20] Navneet Dalal and Bill Triggs. 2005. Histograms of oriented gradients for human detection. In *2005 IEEE computer society conference on computer vision and pattern recognition (CVPR'05)*, Vol. 1. Ieee, 886–893.
- [21] DeepSeek-AI, Aixin Liu, Bei Feng, Bing Xue, Bingxuan Wang, Bochao Wu, Chengda Lu, Chenggang Zhao, Chengqi Deng, Chenyu Zhang, Chong Ruan, Damai Dai, Daya Guo, Dejian Yang, Deli Chen, Dongjie Ji, Erhang Li, Fangyun Lin, Fucang Dai, Fuli Luo, Guangbo Hao, Guanting Chen, Guowei Li, H. Zhang, Han Bao, Hanwei Xu, Haocheng Wang, Haowei Zhang, Honghui Ding, Huajian Xin, Huazuo Gao, Hui Li, Hui Qu, J. L. Cai, Jian Liang, Jianzhong Guo, Jiaqi Ni, Jiashi Li, Jiawei Wang, Jin Chen, Jingchang Chen, Jingyang Yuan, Junjie Qiu, Junlong Li, Junxiao Song, Kai Dong, Kai Hu, Kaige Gao, Kang Guan, Kexin Huang, Kuai Yu, Lean Wang, Lecong Zhang, Lei Xu, Leyi Xia, Liang Zhao, Litong Wang, Liyue Zhang, Meng Li, Miaojun Wang, Mingchuan Zhang, Minghua Zhang, Minghui Tang, Mingming Li, Ning Tian, Panpan Huang, Peiyi Wang, Peng Zhang, Qiancheng Wang, Qihao Zhu, Qinyu Chen, Qiushi Du, R. J. Chen, R. L. Jin, Ruiqi Ge, Ruisong Zhang, Ruizhe Pan, Runji Wang, Runxin Xu, Ruoyu Zhang, Ruyi Chen, S. S. Li, Shanghao Lu, Shangyan Zhou, Shanhuang Chen, Shaoqing Wu, Shengfeng Ye, Shengfeng Ye, Shirong Ma, Shiyu Wang, Shuang Zhou, Shuiping Yu, Shunfeng Zhou, Shutong Pan, T. Wang, Tao Yun, Tian Pei, Tianyu Sun, W. L. Xiao, Wangding Zeng, Wanbiao Zhao, Wei An, Wen Liu, Wenfeng Liang, Wenjun Gao, Wenqin Yu, Wentao Zhang, X. Q. Li, Xiangyue Jin, Xianzu Wang, Xiao Bi, Xiaodong Liu, Xiaohan Wang, Xiaojin Shen, Xiaokang Chen, Xiaokang Zhang, Xiaosha Chen, Xiaotao Nie, Xiaowen Sun, Xiaoxiang Wang, Xin Cheng, Xin Liu, Xin Xie, Xingchao Liu, Xingkai Yu, Xinnan Song, Xinxia Shan, Xinyi Zhou, Xinyu Yang, Xinyuan Li, Xuecheng Su, Xuheng Lin, Y. K. Li, Y. Q. Wang, Y. X. Wei, Y. X. Zhu, Yang Zhang, Yanhong Xu, Yanhong Xu, Yanping Huang, Yao Li, Yao Zhao, Yaofeng Sun, Yaohui Li, Yaohui Wang, Yi Yu, Yi Zheng, Yichao Zhang, Yifan Shi, Yiliang Xiong, Ying He, Ying Tang, Yishi Piao, Yisong Wang, Yixuan Tan, Yiyang Ma, Yiyuan Li, Yongqiang Guo, Yu Wu, Yuan Ou, Yuchen Zhu, Yuduan Wang, Yue Gong, Yuheng Zou, Yujia He, Yukun Zha, Yunfan Xiong, Yuxian Ma, Yuting Yan, Yuxiang Luo, Yuxiang You, Yuxuan Liu, Yuyang Zhou, Z. F. Wu, Z. Z. Ren, Zehui Ren, Zhangli Sha, Zhe Fu, Zhean Xu, Zhen Huang, Zhen Zhang, Zhenda Xie, Zhengyan Zhang, Zhewen Hao, Zhibin Gou, Zhicheng Ma, Zhigang Yan, Zhihong Shao, Zhipeng Xu, Zhiyu Wu, Zhongyu Zhang, Zhuoshu Li, Zihui Gu, Zijia Zhu, Zijun Liu, Zilin Li, Ziwei Xie, Ziyang Song, Ziyi Gao, and Zizheng Pan. 2024. DeepSeek-V3 Technical Report. arXiv:2412.19437 [cs.CL] <https://arxiv.org/abs/2412.19437>
- [22] Yue Fan, Xiaojian Ma, Rujie Wu, Yuntao Du, Jiaqi Li, Zhi Gao, and Qing Li. 2025. Videoagent: A memory-augmented multimodal agent for video understanding. In *European Conference on Computer Vision*. Springer, 75–92.
- [23] Chaoyou Fu, Yuhang Dai, Yondong Luo, Lei Li, Shuhuai Ren, Renrui Zhang, Zihan Wang, Chenyu Zhou, Yunhang Shen, Mengdan Zhang, Peixian Chen, Yanwei Li, Shaohui Lin, Sirui Zhao, Ke Li, Tong Xu, Xiaowu Zheng, Enhong Chen, Rongrong Ji, and Xing Sun. 2024. Video-MME: The First-Ever Comprehensive Evaluation Benchmark of Multi-modal LLMs in Video Analysis. *CoRR* abs/2405.21075 (2024). arXiv:2405.21075 doi:10.48550/ARXIV.2405.21075
- [24] John Gibbs and John Edward Gibbs. 2002. *Mise-en-scène: Film style and interpretation*. Vol. 10. Wallflower Press.
- [25] Qing Guo, Ziyi Cheng, Felix Juefei-Xu, Lei Ma, Xiaofei Xie, Yang Liu, and Jianjun Zhao. 2021. Learning to Adversarially Blur Visual Object Tracking. In *2021 IEEE/CVF International Conference on Computer Vision, ICCV 2021, Montreal, QC, Canada, October 10-17, 2021*. IEEE, 10819–10828. doi:10.1109/ICCV48922.2021.01066

- [26] Jiaming Han, Renrui Zhang, Wenqi Shao, Peng Gao, Peng Xu, Han Xiao, Kaipeng Zhang, Chris Liu, Song Wen, Ziyu Guo, Xudong Lu, Shuai Ren, Yafei Wen, Xiaoxin Chen, Xiangyu Yue, Hongsheng Li, and Yu Qiao. 2023. ImageBind-LLM: Multi-modality Instruction Tuning. *CoRR* abs/2309.03905 (2023). arXiv:2309.03905 doi:10.48550/ARXIV.2309.03905
- [27] Berthold KP Horn and Brian G Schunck. 1981. Determining optical flow. *Artificial intelligence* 17, 1-3 (1981), 185–203.
- [28] Bin Huang, Xin Wang, Hong Chen, Zihan Song, and Wenwu Zhu. 2024. VTimeLLM: Empower LLM to Grasp Video Moments. In *IEEE/CVF Conference on Computer Vision and Pattern Recognition, CVPR 2024, Seattle, WA, USA, June 16-22, 2024*. IEEE, 14271–14280. doi:10.1109/CVPR52733.2024.01353
- [29] Lei Huang, Weijiang Yu, Weitao Ma, Weihong Zhong, Zhangyin Feng, Haotian Wang, Qianglong Chen, Weihua Peng, Xiaocheng Feng, Bing Qin, and Ting Liu. 2023. A Survey on Hallucination in Large Language Models: Principles, Taxonomy, Challenges, and Open Questions. *CoRR* abs/2311.05232 (2023). arXiv:2311.05232 doi:10.48550/ARXIV.2311.05232
- [30] Aaron Hurst, Adam Lerer, Adam P. Goucher, Adam Perelman, Aditya Ramesh, Aidan Clark, AJ Ostrow, Akila Welihinda, Alan Hayes, Alec Radford, Aleksander Madry, Alex Baker-Whitcomb, Alex Beutel, Alex Borzunov, Alex Carney, Alex Chow, Alex Kirillov, Alex Nichol, Alex Paino, Alex Renzin, Alex Tachard Passos, Alexander Kirillov, Alexi Christakis, Alexis Conneau, Ali Kamali, Allan Jabri, Allison Moyer, Allison Tam, Amadou Crookes, Amin Tootoonchian, Ananya Kumar, Andrea Vallone, Andrej Karpathy, Andrew Braunstein, Andrew Cann, Andrew Codispoti, Andrew Galu, Andrew Kondrich, Andrew Tulloch, Andrey Mishchenko, Angela Baek, Angela Jiang, Antoine Pelisse, Antonia Woodford, Anuj Behlolia, Arka Dhar, Ashley Pantuliano, Avi Nayak, Avital Oliver, Barret Zoph, Behrooz Ghorbani, Ben Leimberger, Ben Rossen, Ben Sokolowsky, Ben Wang, Benjamin Zweig, Beth Hoover, Blake Samic, Bob McGrew, Bobby Spero, Bogu Gierlt, Bowen Cheng, Brad Lightcap, Brandon Walkin, Brendan Quinn, Brian Guarraci, Brian Hsu, Bright Kellogg, Brydon Eastman, Camillo Lugaresi, Carroll L. Wainwright, Cary Bassin, Cary Hudson, Casey Chu, Chad Nelson, Chak Li, Chan Jun Shern, Channing Conger, Charlotte Barette, Chelsea Voss, Chen Ding, Cheng Lu, Chong Zhang, Chris Beaumont, Chris Hallacy, Chris Koch, Christian Gibson, Christina Kim, Christine Choi, Christine McLeavey, Christopher Hesse, Claudia Fischer, Clemens Winter, Coley Carnecki, Colin Jarvis, Colin Wei, Constantine Koumouzelis, and Dane Sherburn. 2024. GPT-4o System Card. *CoRR* abs/2410.21276 (2024). arXiv:2410.21276 doi:10.48550/ARXIV.2410.21276
- [31] Ziwei Ji, Nayeon Lee, Rita Frieske, Tiezheng Yu, Dan Su, Yan Xu, Etsuko Ishii, Yejin Bang, Andrea Madotto, and Pascale Fung. 2023. Survey of Hallucination in Natural Language Generation. *ACM Comput. Surv.* 55, 12 (2023), 248:1–248:38. doi:10.1145/3571730
- [32] Raihan Kabir, Naznin Haque, Md. Saiful Islam, and Marium-E-Jannat. 2024. A Comprehensive Survey on Visual Question Answering Datasets and Algorithms. *CoRR* abs/2411.11150 (2024). arXiv:2411.11150 doi:10.48550/ARXIV.2411.11150
- [33] Serpil Kocdar, Nejdet Karadag, and Murat Dogan Sahin. 2016. Analysis of the Difficulty and Discrimination Indices of Multiple-Choice Questions According to Cognitive Levels in an Open and Distance Learning Context. *Turkish Online Journal of Educational Technology-TOJET* 15, 4 (2016), 16–24.
- [34] Woosuk Kwon, Zhuohan Li, Siyuan Zhuang, Ying Sheng, Lianmin Zheng, Cody Hao Yu, Joseph E. Gonzalez, Hao Zhang, and Ion Stoica. 2023. Efficient Memory Management for Large Language Model Serving with PagedAttention. In *Proceedings of the ACM SIGOPS 29th Symposium on Operating Systems Principles*.
- [35] Jie Lei, Licheng Yu, Tamara L. Berg, and Mohit Bansal. 2020. TVQA+: Spatio-Temporal Grounding for Video Question Answering. In *Proceedings of the 58th Annual Meeting of the Association for Computational Linguistics, ACL 2020, Online, July 5-10, 2020*, Dan Jurafsky, Joyce Chai, Natalie Schluter, and Joel R. Tetreault (Eds.). Association for Computational Linguistics, 8211–8225. doi:10.18653/V1/2020.ACL-MAIN.730
- [36] Bo Li, Yuanhan Zhang, Dong Guo, Renrui Zhang, Feng Li, Hao Zhang, Kaichen Zhang, Yanwei Li, Ziwei Liu, and Chunyuan Li. 2024. Llava-onevision: Easy visual task transfer. *arXiv preprint arXiv:2408.03326* (2024).
- [37] Chaoyu Li, Eun Woo Im, and Pooyan Fazli. 2024. VidHalluc: Evaluating Temporal Hallucinations in Multimodal Large Language Models for Video Understanding. arXiv:2412.03735 [cs.CV] <https://arxiv.org/abs/2412.03735>
- [38] Dongxu Li, Yudong Liu, Haoning Wu, Yue Wang, Zhiqi Shen, Bowen Qu, Xinyao Niu, Guoyin Wang, Bei Chen, and Junnan Li. 2024. Aria: An Open Multimodal Native Mixture-of-Experts Model. *arXiv preprint arXiv:2410.05993* (2024).
- [39] Kunhang Li, Yali Wang, Yinan He, Yizhuo Li, Yi Wang, Yi Liu, Zun Wang, Jilan Xu, Guo Chen, Ping Lou, Limin Wang, and Yu Qiao. 2024. MVBench: A Comprehensive Multi-modal Video Understanding Benchmark. In *IEEE/CVF Conference on Computer Vision and Pattern Recognition, CVPR 2024, Seattle, WA, USA, June 16-22, 2024*. IEEE, 22195–22206. doi:10.1109/CVPR52733.2024.02095
- [40] Yifan Li, Yifan Du, Kun Zhou, Jinpeng Wang, Wayne Xin Zhao, and Ji-Rong Wen. 2023. Evaluating Object Hallucination in Large Vision-Language Models. In *Proceedings of the 2023 Conference on Empirical Methods in Natural Language Processing, EMNLP 2023, Singapore, December 6-10, 2023*, Houda Bouamor, Juan Pino, and Kalika Bali (Eds.). Association for Computational Linguistics, 292–305. doi:10.18653/V1/2023.EMNLP-MAIN.20
- [41] Yanyang Li, Shuo Liang, Michael R Lyu, and Liwei Wang. 2024. Making long-context language models better multi-hop reasoners. *arXiv preprint arXiv:2408.03246* (2024).
- [42] Yanwei Li, Chengyao Wang, and Jiaya Jia. 2025. Llama-vid: An image is worth 2 tokens in large language models. In *European Conference on Computer Vision*. Springer, 323–340.
- [43] Bin Lin, Yang Ye, Bin Zhu, Jiaxi Cui, Munan Ning, Peng Jin, and Li Yuan. 2024. Video-LLaVA: Learning United Visual Representation by Alignment Before Projection. In *Proceedings of the 2024 Conference on Empirical Methods in Natural Language Processing, EMNLP 2024, Miami, FL, USA, November 12-16, 2024*, Yaser Al-Onaizan, Mohit Bansal, and Yun-Nung Chen (Eds.). Association for Computational Linguistics, 5971–5984. doi:10.18653/V1/2024.EMNLP-MAIN.342
- [44] Ji Lin, Hongxu Yin, Wei Ping, Yao Lu, Pavlo Molchanov, Andrew Tao, Huizi Mao, Jan Kautz, Mohammad Shoeybi, and Song Han. 2023. VILA: On Pre-training for Visual Language Models. arXiv:2312.07533 [cs.CV]
- [45] Kevin Lin, Faisal Ahmed, Linjie Li, Chung-Ching Lin, Ehsan Azarnasab, Zhengyuan Yang, Jianfeng Wang, Lin Liang, Zicheng Liu, Yumao Lu, Ce Liu, and Lijuan Wang. 2023. MM-VID: Advancing Video Understanding with GPT-4V(ision). *CoRR* abs/2310.19773 (2023). arXiv:2310.19773 doi:10.48550/ARXIV.2310.19773
- [46] Tsung-Yi Lin, Michael Maire, Serge J. Belongie, James Hays, Pietro Perona, Deva Ramanan, Piotr Dollár, and C. Lawrence Zitnick. 2014. Microsoft COCO: Common Objects in Context. In *Computer Vision - ECCV 2014 - 13th European Conference, Zurich, Switzerland, September 6-12, 2014, Proceedings, Part V (Lecture Notes in Computer Science, Vol. 8693)*, David J. Fleet, Tomás Pajdla, Bernt Schiele, and Tinne Tuytelaars (Eds.). Springer, 740–755. doi:10.1007/978-3-319-10602-1_48
- [47] Yuanze Lin, Xun Guo, and Yan Lu. 2021. Self-Supervised Video Representation Learning with Meta-Contrastive Network. In *2021 IEEE/CVF International Conference on Computer Vision, ICCV 2021, Montreal, QC, Canada, October 10-17, 2021*. IEEE, 8219–8229. doi:10.1109/ICCV48922.2021.00813
- [48] Fuxiao Liu, Tianrui Guan, Zongxia Li, Lichang Chen, Yaser Yacoob, Dinesh Manocha, and Tianyi Zhou. 2023. HallusionBench: You See What You Think? Or You Think What You See? An Image-Context Reasoning Benchmark Challenging for GPT-4V(ision), LLaVA-1.5, and Other Multi-modality Models. *CoRR* abs/2310.14566 (2023). arXiv:2310.14566 doi:10.48550/ARXIV.2310.14566
- [49] Jiazhen Liu, Yuhao Fu, Ruobing Xie, Runquan Xie, Xingwu Sun, Fengzong Lian, Zhanhui Kang, and Xirong Li. 2024. PhD: A Prompted Visual Hallucination Evaluation Dataset. *CoRR* abs/2403.11116 (2024). arXiv:2403.11116 doi:10.48550/ARXIV.2403.11116
- [50] Yuanxin Liu, Shicheng Li, Yi Liu, Yuxiang Wang, Shuhuai Ren, Lei Li, Sishuo Chen, Xu Sun, and Lu Hou. 2024. TempCompass: Do Video LLMs Really Understand Videos?. In *Findings of the Association for Computational Linguistics, ACL 2024, Bangkok, Thailand and virtual meeting, August 11-16, 2024*, Lun-Wei Ku, Andre Martins, and Vivek Srikumar (Eds.). Association for Computational Linguistics, 8731–8772. doi:10.18653/V1/2024.FINDINGS-ACL.517
- [51] Zuyan Liu, Yuhao Dong, Ziwei Liu, Winston Hu, Jiwen Lu, and Yongming Rao. 2024. Oryx MLLM: On-Demand Spatial-Temporal Understanding at Arbitrary Resolution. *arXiv preprint arXiv:2409.12961* (2024).
- [52] Kaili Ma, Garry Yang, Han Yang, Yongqiang Chen, and James Cheng. 2023. Calibrating and Improving Graph Contrastive Learning. *Trans. Mach. Learn. Res.* 2023 (2023). <https://openreview.net/forum?id=LdSP6cvTS4>
- [53] Neelu Madan, Andreas Møgelmoose, Rajat Modi, Yogesh S. Rawat, and Thomas B. Moeslund. 2024. Foundation Models for Video Understanding: A Survey. *CoRR* abs/2405.03770 (2024). arXiv:2405.03770 doi:10.48550/ARXIV.2405.03770
- [54] Matei Mancas, Vincent P Ferrera, Nicolas Riche, and John G Taylor. 2016. *From Human Attention to Computational Attention*. Vol. 2. Springer.
- [55] Mayug Maniparambil, Raiymbek Akshulakov, Yasser Abdelaziz Dahou Djilali, Mohamed El Amine Seddik, Sanath Narayan, Kartikeya Mangalam, and Noel E. O'Connor. 2024. Do Vision and Language Encoders Represent the World Similarly?. In *IEEE/CVF Conference on Computer Vision and Pattern Recognition, CVPR 2024, Seattle, WA, USA, June 16-22, 2024*. IEEE, 14334–14343. doi:10.1109/CVPR52733.2024.01359
- [56] Christopher Manning and Hinrich Schütze. 1999. *Foundations of statistical natural language processing*. MIT press.
- [57] Shervin Minaee, Tomás Mikolov, Narjes Nikzad, Meysam Chenaghlu, Richard Socher, Xavier Amatriain, and Jianfeng Gao. 2024. Large Language Models: A Survey. *CoRR* abs/2402.06196 (2024). arXiv:2402.06196 doi:10.48550/ARXIV.2402.06196
- [58] Thong Nguyen, Yi Bin, Junbin Xiao, Leigang Qu, Yicong Li, Jay Zhangjie Wu, Cong-Duy Nguyen, See-Kiong Ng, and Anh Tuan Luu. 2024. Video-Language Understanding: A Survey from Model Architecture, Model Training, and Data Perspectives. In *Findings of the Association for Computational Linguistics, ACL 2024, Bangkok, Thailand and virtual meeting, August 11-16, 2024*, Lun-Wei Ku, Andre Martins, and Vivek Srikumar (Eds.). Association for Computational Linguistics, 3636–3657. doi:10.18653/V1/2024.FINDINGS-ACL.217
- [59] Munan Ning, Bin Zhu, Yujia Xie, Bin Lin, Jiaxi Cui, Lu Yuan, Dongdong Chen, and Li Yuan. 2023. Video-Bench: A Comprehensive Benchmark and Toolkit for

- Evaluating Video-based Large Language Models. *CoRR* abs/2311.16103 (2023). arXiv:2311.16103 doi:10.48550/ARXIV.2311.16103
- [60] OpenAI. 2023. GPT-4 Technical Report. *CoRR* abs/2303.08774 (2023). arXiv:2303.08774 doi:10.48550/ARXIV.2303.08774
- [61] Viorica Patraucean, Lucas Smaira, Ankush Gupta, Adrià Recasens, Larisa Markeeva, Dylan Banarse, Skanda Koppula, Joseph Heyward, Mateusz Malinowski, Yi Yang, Carl Doersch, Tatiana Matejovicova, Yury Sulsky, Antoine Miech, Alexandre Fréchet, Hanna Klimczak, Raphael Koster, Junlin Zhang, Stephanie Winkler, Yusuf Aytar, Simon Osindero, Dima Damen, Andrew Zisserman, and João Carreira. 2023. Perception Test: A Diagnostic Benchmark for Multimodal Video Models. In *Advances in Neural Information Processing Systems 36: Annual Conference on Neural Information Processing Systems 2023, NeurIPS 2023, New Orleans, LA, USA, December 10 - 16, 2023*, Alice Oh, Tristan Naumann, Amir Globerson, Kate Saenko, Moritz Hardt, and Sergey Levine (Eds.). http://papers.nips.cc/paper_files/paper/2023/hash/8540fba4abdc7f9f7a7b1cc6cd60e409-Abstract-Datasets_and_Benchmarks.html
- [62] Alec Radford, Jong Wook Kim, Chris Hallacy, Aditya Ramesh, Gabriel Goh, Sandhini Agarwal, Girish Sastry, Amanda Askell, Pamela Mishkin, Jack Clark, Gretchen Krueger, and Ilya Sutskever. 2021. Learning Transferable Visual Models From Natural Language Supervision. In *Proceedings of the 38th International Conference on Machine Learning, ICM 2021, 18-24 July 2021, Virtual Event (Proceedings of Machine Learning Research, Vol. 139)*, Marina Meila and Tong Zhang (Eds.). PMLR, 8748–8763. <http://proceedings.mlr.press/v139/radford21a.html>
- [63] Joseph Redmon, Santosh Kumar Divvala, Ross B. Girshick, and Ali Farhadi. 2016. You Only Look Once: Unified, Real-Time Object Detection. In *2016 IEEE Conference on Computer Vision and Pattern Recognition, CVPR 2016, Las Vegas, NV, USA, June 27-30, 2016*. IEEE Computer Society, 779–788. doi:10.1109/CVPR.2016.91
- [64] G. Rose. 2007. *Visual Methodologies: An Introduction to the Interpretation of Visual Materials*. SAGE Publications. <https://books.google.com.hk/books?id=gnUPNcnYjIC>
- [65] Pranab Sahoo, Prabhaskar Meheria, Akash Ghosh, Sriparna Saha, Vinija Jain, and Aman Chadha. 2024. A Comprehensive Survey of Hallucination in Large Language, Image, Video and Audio Foundation Models. In *Findings of the Association for Computational Linguistics: EMNLP 2024, Miami, Florida, USA, November 12-16, 2024*, Yaser Al-Onaizan, Mohit Bansal, and Yun-Nung Chen (Eds.). Association for Computational Linguistics, 11709–11724. <https://aclanthology.org/2024.findings-emnlp.685>
- [66] Pranab Sahoo, Prabhaskar Meheria, Akash Ghosh, Sriparna Saha, Vinija Jain, and Aman Chadha. 2024. Unveiling Hallucination in Text, Image, Video, and Audio Foundation Models: A Comprehensive Survey. *CoRR* abs/2405.09589 (2024). arXiv:2405.09589 doi:10.48550/ARXIV.2405.09589
- [67] Darshana Saravanan, Darshan Singh S, Varun Gupta, Zeeshan Khan, Vineet Gandhi, and Makarand Tapaswi. 2024. VELOCITI: Can Video-Language Models Bind Semantic Concepts through Time? *CoRR* abs/2406.10889 (2024). arXiv:2406.10889 doi:10.48550/ARXIV.2406.10889
- [68] Yan Shu, Peitian Zhang, Zheng Liu, Minghao Qin, Junjie Zhou, Tiejun Huang, and Bo Zhao. 2024. Video-xl: Extra-long vision language model for hour-scale video understanding. *arXiv preprint arXiv:2409.14485* (2024).
- [69] Khurram Soomro, Amir Roshan Zamir, and Mubarak Shah. 2012. UCF101: A Dataset of 101 Human Actions Classes From Videos in The Wild. *CoRR* abs/1212.0402 (2012). arXiv:1212.0402 <http://arxiv.org/abs/1212.0402>
- [70] Khurram Soomro, Amir Roshan Zamir, and Mubarak Shah. 2012. UCF101: A Dataset of 101 Human Actions Classes From Videos in The Wild. arXiv:1212.0402 [cs.CV] <https://arxiv.org/abs/1212.0402>
- [71] Matteo Stefanini, Marcella Cornia, Lorenzo Baraldi, Silvia Cascianelli, Giuseppe Fiameni, and Rita Cucchiara. 2023. From Show to Tell: A Survey on Deep Learning-Based Image Captioning. *IEEE Trans. Pattern Anal. Mach. Intell.* 45, 1 (2023), 539–559. doi:10.1109/TPAMI.2022.3148210
- [72] Yunlong Tang, Jing Bi, Siting Xu, Luchuan Song, Susan Liang, Teng Wang, Daoan Zhang, Jie An, Jingyang Lin, Rongyi Zhu, Ali Vosoughi, Chao Huang, Zeliang Zhang, Feng Zheng, Jianguo Zhang, Ping Luo, Jiebo Luo, and Chenliang Xu. 2023. Video Understanding with Large Language Models: A Survey. *CoRR* abs/2312.17432 (2023). arXiv:2312.17432 doi:10.48550/ARXIV.2312.17432
- [73] Gemini Team, Petko Georgiev, Ving Ian Lei, Ryan Burnell, Libin Bai, Anmol Gulati, Garrett Tanzer, Damien Vincent, Zhufeng Pan, Shibo Wang, et al. 2024. Gemini 1.5: Unlocking multimodal understanding across millions of tokens of context. *arXiv preprint arXiv:2403.05530* (2024).
- [74] Jean-Philippe Thiran, Ferran Marques, and Hervé Bourlard. 2009. *Multimodal Signal Processing: Theory and applications for human-computer interaction*. Academic Press.
- [75] Hugo Touvron, Thibaut Lavril, Gautier Izacard, Xavier Martinet, Marie-Anne Lachaux, Timothée Lacroix, Baptiste Rozière, Naman Goyal, Eric Hambro, Faisal Azhar, Aurélien Rodriguez, Armand Joulin, Edouard Grave, and Guillaume Lample. 2023. LLaMA: Open and Efficient Foundation Language Models. *CoRR* abs/2302.13971 (2023). arXiv:2302.13971 doi:10.48550/ARXIV.2302.13971
- [76] Carol Vernallis, Amy Herzog, and John Richardson. 2013. *The Oxford handbook of sound and image in digital media*. OUP USA.
- [77] Peng Wang, Shuai Bai, Sinan Tan, Shijie Wang, Zhihao Fan, Jinze Bai, Keqin Chen, Xuejing Liu, Jialin Wang, Wenbin Ge, Yang Fan, Kai Dang, Mengfei Du, Xuancheng Ren, Rui Men, Dayiheng Liu, Chang Zhou, Jingren Zhou, and Junyang Lin. 2024. Qwen2-VL: Enhancing Vision-Language Model’s Perception of the World at Any Resolution. arXiv:2409.12191 [cs.CV] <https://arxiv.org/abs/2409.12191>
- [78] Yuxuan Wang, Yueqian Wang, Dongyan Zhao, Cihang Xie, and Zilong Zheng. 2024. VideoHalluciner: Evaluating Intrinsic and Extrinsic Hallucinations in Large Video-Language Models. *CoRR* abs/2406.16338 (2024). arXiv:2406.16338 doi:10.48550/ARXIV.2406.16338
- [79] T Wolf. 2019. Huggingface’s transformers: State-of-the-art natural language processing. *arXiv preprint arXiv:1910.03771* (2019).
- [80] Chenyu Yang, Xuan Dong, Xizhou Zhu, Weijie Su, Jiahao Wang, Hao Tian, Zhe Chen, Wenhai Wang, Lewei Lu, and Jifeng Dai. 2024. PVC: Progressive Visual Token Compression for Unified Image and Video Processing in Large Vision-Language Models. arXiv:2412.09613 [cs.CV] <https://arxiv.org/abs/2412.09613>
- [81] Dongjie Yang, Suyuan Huang, Chengqiang Lu, Xiaodong Han, Haoxin Zhang, Yan Gao, Yao Hu, and Hai Zhao. 2024. Vript: A Video Is Worth Thousands of Words. *CoRR* abs/2406.06040 (2024). arXiv:2406.06040 doi:10.48550/ARXIV.2406.06040
- [82] Shukang Yin, Chaoyou Fu, Sirui Zhao, Ke Li, Xing Sun, Tong Xu, and En-hong Chen. 2023. A Survey on Multimodal Large Language Models. *CoRR* abs/2306.13549 (2023). arXiv:2306.13549 doi:10.48550/ARXIV.2306.13549
- [83] Jingyi Zhang, Jiaxing Huang, Sheng Jin, and Shijian Lu. 2024. Vision-Language Models for Vision Tasks: A Survey. *IEEE Trans. Pattern Anal. Mach. Intell.* 46, 8 (2024), 5625–5644. doi:10.1109/TPAMI.2024.3369699
- [84] Jiacheng Zhang, Yang Jiao, Shaoxiang Chen, Jingjing Chen, and Yu-Gang Jiang. 2024. EventHallusion: Diagnosing Event Hallucinations in Video LLMs. *CoRR* abs/2409.16597 (2024). arXiv:2409.16597 doi:10.48550/ARXIV.2409.16597
- [85] Yuanhan Zhang, Bo Li, haotian Liu, Yong jae Lee, Liangkai Gui, Di Fu, Jiashi Feng, Ziwei Liu, and Chunyuan Li. 2024. LLaVA-NeXT: A Strong Zero-shot Video Understanding Model. <https://llava-vl.github.io/blog/2024-04-30-llava-next-video/>
- [86] Yuanhan Zhang, Jinming Wu, Wei Li, Bo Li, Zejun Ma, Ziwei Liu, and Chunyuan Li. 2024. Video Instruction Tuning With Synthetic Data. arXiv:2410.02713 [cs.CV] <https://arxiv.org/abs/2410.02713>
- [87] Yudong Zhang, Ruobing Xie, Jiansheng Chen, Xingwu Sun, Zhanhui kang, and Yu Wang. 2024. DHCP: Detecting Hallucinations by Cross-modal Attention Pattern in Large Vision-Language Models. *CoRR* abs/2411.18659 (2024). arXiv:2411.18659 doi:10.48550/ARXIV.2411.18659
- [88] Junjie Zhou, Yan Shu, Bo Zhao, Boya Wu, Zhengyang Liang, Shitao Xiao, Minghao Qin, Xi Yang, Yongping Xiong, Bo Zhang, Tiejun Huang, and Zheng Liu. 2025. MLVU: Benchmarking Multi-task Long Video Understanding. arXiv:2406.04264 [cs.CV] <https://arxiv.org/abs/2406.04264>

A Human understanding videos

Video, first captured and screened by the Lumière brothers in the late 19th century, evolved from silent image sequences to include sound, enhancing its multimodal nature [76]. Video understanding, as a methodology combining visual, auditory, and temporal elements, has evolved significantly over time. Research has primarily focused on processing and interpreting these modalities by humans and machines [72, 74, 83]. Our benchmark specifically examines human understanding of the visual components of videos, excluding audio. It focuses on *mise-en-scène*, which refers to all elements captured in videos [7, 24]. In video comprehension, *mise-en-scène* is categorized into three domains: **setting**, **people and their appearance** (e.g., clothing, makeup), and **stage** (e.g., actions, talking).

- **Setting** refers to the physical location where the video takes place, as well as the objects present within the scene. These settings provide crucial context for understanding the narrative and the relationships between people and their environment [5, 7].
- **People and Their Appearance** involve the individuals featured in the video, with particular attention to their physical characteristics, gender, clothing, and makeup. These elements contribute to the portrayal of their identity [24].
- **Stage** encompasses the actions and movements of both the characters and objects within the scene, including conversations, which require the integration of temporal information to understand the sequence of events. The dynamic nature of these is critical in establishing the progression flow of video contents [5].

Human perception of video content typically follows a process in which the viewer first identifies the environment and objects in the opening frame [7, 24]. Attention is often directed toward the people featured in the scene, particularly their appearance and behaviors [6]. As the video progresses, viewers become attuned to changes in subsequent frames, identifying who is delivering words and subtle shifts that introduce new information or obscure prior details. This process of dynamic attention and interpretation aligns with the principles of human video comprehension [16, 54]. The dataset developed for our study is designed to assess the ability of LVLMs in avoiding hallucination results to replicate these aspects of human video understanding. By focusing on the elements of *mise-en-scène*, we aim to evaluate how effectively LVLMs can recognize and process the visual components that humans instinctively interpret when viewing videos.

B MESH Benchmark

B.1 Metric



Figure 9: Left: "A man wearing long-sleeved collared pink button-up shirt with pockets and not wearing glasses appears in the video". Right: "A man wearing a gray jacket picks up his napkin under the table".

B.1.1 Why using multi-choice questions?

Efficiency. Multi-choice questions offer enhanced efficiency in evaluation by aggregating more information per question compared to binary formats. While binary questions assess a single statement about the video, multi-choice questions can simultaneously examine a model’s understanding across multiple facets of the video content through a single question. Considering the substantial computational cost associated with LVLM inference, and recognizing that current LVLM architectures and implementations [18, 34, 79] often face limitations in handling the extensive context length required for processing long-form video content, minimizing the total number of questions becomes paramount. Therefore, the ability of multi-choice questions to consolidate assessment points significantly reduces the overall resource expenditure and time required for comprehensive evaluation.

Clarity. Binary questions are inherently susceptible to ambiguity, posing challenges for precise LVLM evaluation. One primary source of ambiguity stems from the interpretation of features, particularly when moving beyond basic object recognition. Empirical evidence suggests that object recognition benchmarks are approaching saturation for advanced LVLMs, necessitating the use of finer-grained features to discern subtle differences in model performance. However, describing these more nuanced features often introduces ambiguity. For example, consider the statement about the pink shirt (Figure 9 left). While the dominant color is demonstrably pink, one could argue that the presence of gray and black threads undermines the statement’s precision, making its binary correctness debatable. Another source of

ambiguity arises from the inherent nature of LVLMs and their reliance on frame sampling for video understanding. This sampling can lead to a lack of perceived motion continuity, creating ambiguity in action interpretation. In the napkin example (Figure 9 right), the statement implies a self-initiated action, yet the limited temporal resolution could equally support interpretations of the man receiving the napkin from another person. Such ambiguities render the accuracy of binary tasks susceptible to subjective interpretations, potentially obscuring the objective evaluation of the LVLM’s abilities. In contrast, the inherently contrastive nature of multi-choice questions mitigates this issue. By requiring models to select the most appropriate statement from a set of options, rather than judging absolute correctness, multi-choice questions reduce the impact of subjective interpretations and focus the evaluation on comparative understanding.

Discrimination. In binary question formats, the potential range of accuracy scores for a model is limited, theoretically spanning from chance performance (50%) to perfect accuracy (100%). This restricted range limits the ability to effectively differentiate between models with similar performance. When models exhibit closely aligned performance on binary tasks, their scores become nearly indistinguishable within this narrow interval, and accuracy measurements become more susceptible to the influence of random noise and minor variations in question design. In contrast, for multi-choice questions with ‘n’ options, the theoretical accuracy range expands significantly, from chance performance (approximately $100\%/n$) to perfect accuracy (100%). This broader spectrum of possible accuracy scores provides a greater capacity to discern subtle performance differences between models and reduces the relative impact of random fluctuations, leading to a more robust and reliable evaluation of LVLM capabilities.

B.1.2 Additional metric: JSD. In the following detailed results, we further employ Jensen-Shannon Divergence (JSD) [56] to measure the option distribution between ground-truth and prediction. We have

$$JS(P\|Q) = \frac{1}{2} \sum_x P(x) \ln \frac{P(x)}{M(x)} + \frac{1}{2} \sum_x Q(x) \ln \frac{Q(x)}{M(x)},$$

where $M(x) = \frac{1}{2}(P(x) + Q(x))$. Here, $P(x)$ represents the ground-truth distribution, and $Q(x)$ represents the predicted distribution. For binary tasks, $x \in \{\text{"yes"}, \text{"no"}\}$, while for multiple-choice tasks, $x \in \{A, B, C, D\}$. We normalize the JSD for the binary task by dividing by 0.216 and for the MC task by dividing by 0.38.

B.2 Setting hallucination

B.2.1 Uniqueness of Setting. Unlike image datasets like MSCOCO [46], where annotated objects are present in nearly all frames, video annotations often miss objects in many frames. Motion blur and the complexity of real-world scenarios further complicate annotating all objects within a single frame [1, 25], making manual annotation both costly and time-intensive. As discussed in Section A and Appendix A, humans comprehend videos by first identifying environments through object sets. For instance, in Figure 3, items like wineglasses, flowers, and plates provide context about the setting, which influences our overall understanding of subsequent frames. To address sparse object annotations and leverage environment labels, we associate unique object sets with their corresponding environments.

B.2.2 Object Annotation. The object names depicted in the video clips are extracted from the TVQA+ dataset utilizing Deepseek-v3 [21]. Spatial grounding information within the TVQA+ dataset is leveraged to procure object names within the video content that are lifeless and discernible, such as "bed," while excluding terms like "mass," "mother," and "melting." In order to enhance the efficacy of the LLM, a comparative approach is employed for the extraction process. The methodology details and an example are presented in Table 8 and Algorithm 1.

Algorithm 1 Object Annotation Filter

Input: Video v_i ’s object annotation set $S_o = \{o_1, o_2, \dots, o_n\}$

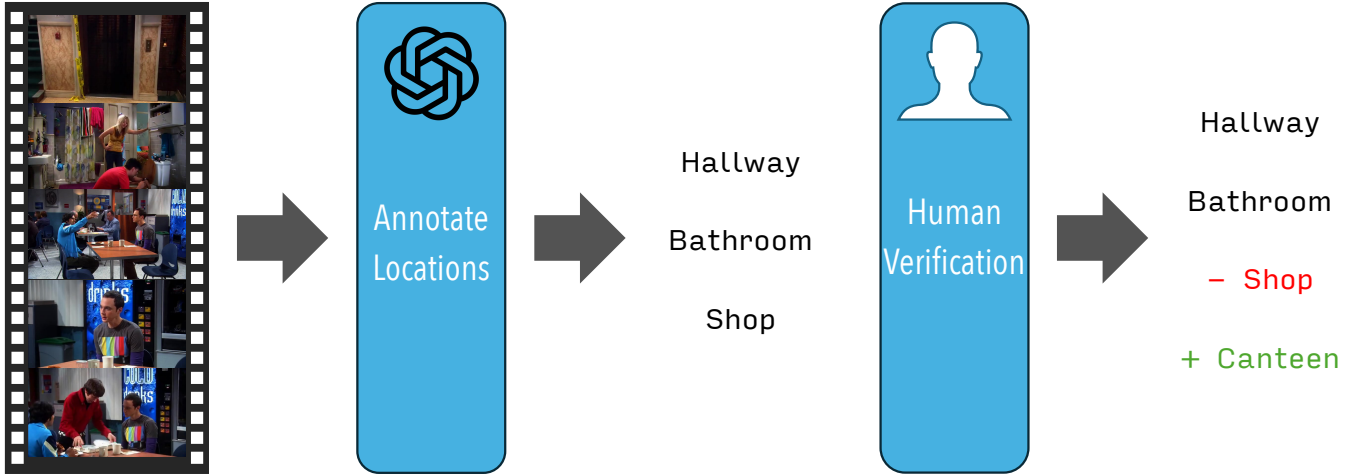
- 1: $A_o \leftarrow [o_r, o_1, o_2, \dots, o_n]$, where o_r is the reference object.
- 2: $A_o \leftarrow \text{LLM}(\text{"... Sort the list by visibility and materiality of each element in } A_o \text{ ..."})$
- 3: $I_r \leftarrow \text{index}(A_o, o_r)$.
- 4: $S_{o_{target}} \leftarrow A_o[I_r]$

Output: Target object set $S_{o_{target}} = \{o_{1'}, o_{2'}, \dots, o_{n'}\}$

B.2.3 Selecting Setting. The location of the scene within each video clip is extracted utilizing Int4 quantization version of LVM Qwen2-VL [77]. To account for potential variations in naming and hallucination output, human annotators unify names and correct the wrong content. This process is shown in Figure 11. For each extracted object and its corresponding location, a location that appears in other video clips but not in the current one is selected. Subsequently, an open source LLM DeepSeek-v3 [21] is employed to identify five objects that are only present in the chosen location. These five objects are then used to formulate questions that inquire about the existence of objects not present in the scene. As Figure 10 shows, in the video clip **A**, the only visible scene is a living room containing a chair. By contrast, the classroom scene appears in clip **B** but not in clip **A**. To identify objects that are typically found in classrooms but rarely in living rooms, LLM is queried and it generates terms such as "whiteboard" and "teacher’s podium," which align with the specified criteria. The details are presented in Algorithm 2.

Table 8: Concrete Example of Object Annotation Filter.

Step	Procedure	Resultant State
1	Video v_i 's object annotation set	Original set: {Crowd, Mass, Football}
2	Introduce the reference object <i>Pepper</i> to the list.	Augmented list: [Crowd, Mass, Football, Pepper]
3	Invoke the LLM to rank objects by the visibility and materiality .	LLM-sorted list: [Football, Pepper, Mass, Crowd]
4	Identify the index of <i>Pepper</i> and prune all terms behind the index.	Post-pruning set: {Football}

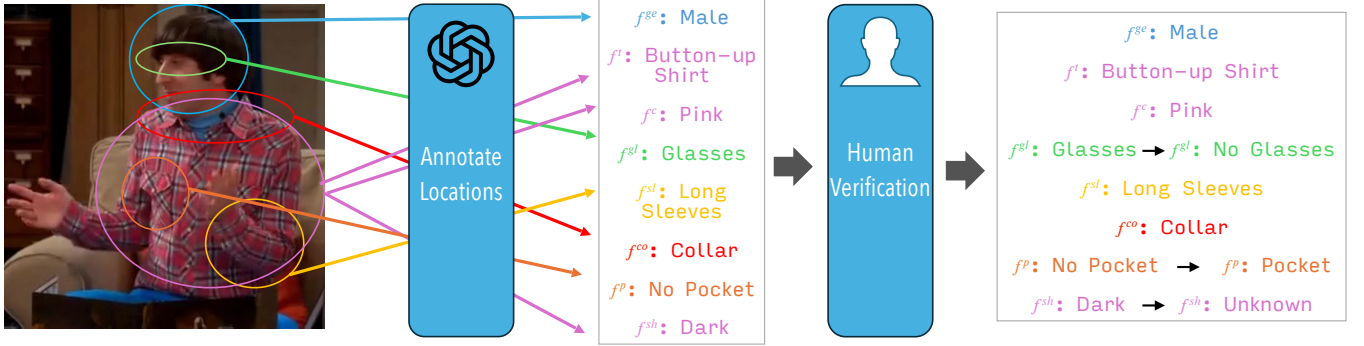
**Figure 10: Left: Representative frame from clip A depicting A domestic living room environment, Right: Representative frame from clip B illustrating a classroom setting.****Figure 11: Pipeline for labeling the locations in the video.**

B.3 Character hallucination

B.3.1 Uniqueness of Character. As discussed in Appendix A, characters have been central to most videos since the medium’s inception, despite their lower average density compared to objects. Videos primarily convey information through human appearances and movements [7, 24]. In videos, characters naturally and dynamically appear and disappear (cut-ins and cut-offs) throughout videos. Moreover, a single video often features multiple characters, not all of whom appear in any single frame. For instance, in Figure 4, four individuals are present, but no frame contains all of them simultaneously. Identifying the unique features of each character within a video forms the foundation for deeper comprehension.

Algorithm 2 Trap Objects Selection

Input: Video v_i 's location annotation set $S_L = \{L_1, L_2, \dots, L_n\}$, Location set \mathbb{L} that contains all possible locations, Number of iteration n_t .
 1: **for** iteration = 1, 2, ..., n_t **do** ▷ Outer Loop
 2: $L_{trap} \leftarrow \text{random}(\mathbb{L})$.
 3: **for** L_j in $\{L_1, L_2, \dots, L_n\}$ **do**
 4: **if** $L_j \approx L_{trap}$ **then**
 5: Continue the Outer Loop.
 6: **end if**
 7: **end for**
 8: $o_{trap} \leftarrow \text{LLM}(\text{"...Choose objects (if exist) that is possible to appear in } L_{trap} \text{ but never appear in } L_1, L_2, \dots, \text{ and } L_n \dots")$
 9: **end for**
Output: Trap object set $S_{o_{trap}} = \{o_{trap_1}, o_{trap_2}, \dots, o_{trap_n}\}$

**Figure 12: Pipeline for labeling the character features in the video.****Algorithm 3** Person Hallucination Questions Construction

Input: v_i 's person set $S_P = \{P_1, P_2, \dots, P_n\}$, Feature pool $[\mathbb{F}^{ge}, \mathbb{F}^t, \mathbb{F}^c, \mathbb{F}^{gl}, \mathbb{F}^{sl}, \mathbb{F}^{co}, \mathbb{F}^p, \mathbb{F}^{sh}]$, Granularity mask $M = [m^{ge}, m^t, m^c, m^{gl}, m^{sl}, m^{co}, m^p, m^{sh}]$, Number of Iteration n_t .
 1: **for** P_j in $S_P = \{P_1, P_2, \dots, P_n\}$ **do**
 2: $P_j \leftarrow M \star P_j$
 3: **end for**
 4: **for** iteration = 1, 2, ..., n_t **do** ▷ Loop 1
 5: $P_{trap} \leftarrow \text{random}(S_P)$.
 6: **for** f_{trap}^j in $P_{trap} = [\mathbb{F}_{trap}^{ge}, \mathbb{F}_{trap}^t, \mathbb{F}_{trap}^c, \mathbb{F}_{trap}^{gl}, \mathbb{F}_{trap}^{sl}, \mathbb{F}_{trap}^{co}, \mathbb{F}_{trap}^p, \mathbb{F}_{trap}^{sh}]$ **do**
 7: **if** f_{trap}^j is not masked **then**
 8: $f_{trap}^j \leftarrow \text{random}(\mathbb{F}^j)$
 9: **end if**
 10: **end for**
 11: **for** P_k in $S_P = \{P_1, P_2, \dots, P_n\}$ **do** ▷ Loop 2
 12: **for** f_k^j in $P_k = [\mathbb{F}_k^{ge}, \mathbb{F}_k^t, \mathbb{F}_k^c, \mathbb{F}_k^{gl}, \mathbb{F}_k^{sl}, \mathbb{F}_k^{co}, \mathbb{F}_k^p, \mathbb{F}_k^{sh}]$ **do**
 13: **if** $f_{trap}^j \neq f_k^j$ **then**
 14: Continue the Loop 2
 15: **end if**
 16: Continue the Loop 1
 17: **end for**
 18: **end for**
 19: **end for**
Output: Target person set $S_{P_{target}} = \{P_1, P_2, \dots, P_n\}$, Trap person set $S_{P_{trap}} = \{P_{trap_1}, P_{trap_2}, \dots, P_{trap_n}\}$

B.3.2 Generating character features. In the process of feature extraction, spatial grounding information sourced from the TVQA+ dataset is utilized in conjunction with Deepseek-v3 [21] and GPT-4o [30]. Initially, individual name and their corresponding frame-level bounding boxes are derived from the spatial grounding information employing Deepseek-v3. Subsequently, by leveraging the extracted names and bounding box specifics, eight distinctive person features are generated by GPT-4o, containing the following attributes:

- **Garment Type:** e.g., t-shirt, jacket, coat, button-up shirt, blouse, etc.
- **Garment Color:** e.g., red, blue, yellow, green, etc.
- **Gender:** Male or female.
- **Glasses:** Whether the person wears glasses or not.
- **Garment Sleeve:** e.g., long sleeves, short sleeves, no sleeves, and half sleeves.
- **Garment Collar:** Whether the upper garment has a collar or not.
- **Garment Pocket:** Whether the upper garment has pockets or not.
- **Garment Shade:** Whether the overall color of the upper garment is dark or light.

Following the feature extraction phase, a human verification stage is conducted on the dataset. These eight discriminative features are employed to denote an individual in the video, as exemplified by Sheldon’s feature set in video clip **A** (Figure 10): {"Garment Type": "t-shirt", "Garment Color": "blue", "Gender": "male", "Glasses": "no glasses", "Garment Sleeve": "short sleeves", "Garment Collar": "no collar", "Garment Pocket": "no pocket", "Garment Shade": "unknown"}. Each character feature goes through a human verification process as illustrated in Figure 12.

B.3.3 Selecting Character. To construct the targets with different granularity in Binary Task and MC Task, undesired features are masked by Granularity Mask M , the desired features are formulated anonymous descriptors (e.g., "A male wearing a blue t-shirt" or "A person in short-sleeved blue upper garment without glasses") to indicate Sheldon in the video clip, replacing direct name references "Sheldon".

To construct high-quality traps, for each category of person-related features, human annotators manually cluster semantically similar attributes into taxonomically organized groups. For instance, within the "Garment Type" classification, items such as button-up shirts and long-sleeved shirts are aggregated into a unified semantic category. During the generation of traps, for every character in the video clips, his/her features are replaced with alternative attributes from distinct categorical groups of the same feature type to form the trap character in the question. This mechanism is denoted by operation " \neq " in Algorithm 3. It generates traps that can be clearly distinguished from the original character, instead of simply "rephrasing" the features. The formal construction process is listed in Algorithm 3.

The detailed information of each subdataset with different granularity is listed below:

- **Coarse-Grained Subdataset:** This subdataset is constructed using the three most visually distinguishable features: **Garment Type**, **Garment Color**, and **Gender**, with undesired features like **Glasses** and **Garment Sleeve** being masked. These features serve as the primary identifiers for each individual within the subdataset. *Example:* {"Garment Color": "green", "Garment Type": "t-shirt", "Gender": "female"} is transformed to "a woman wearing green t-shirt".
- **Medium-Grained Subdataset:** Building upon the Coarse-Grained Subdataset, this version un.masks two additional, less prominent features: **Glasses** and **Garment Sleeve**. *Example:* {"Garment Color": "white", "Garment Type": "coat", "Glasses": "no glasses", "Garment Sleeve": "long sleeves", "Gender": "male"} is converted to "a man wearing long-sleeved white coat and not wearing glasses".
- **Mixed-Grained Subdataset:** In comparison to the Medium-Grained Subdataset, three additional, less noticeable features are un.masks: **Garment Collar**, **Garment Pocket**, and **Garment Shade**, resulting in a total of eight features. To assess the model’s robustness against missing information, three out of the eight available features are randomly selected to be masked. *Example:* {"Garment Color": "red", "Garment Shade": "unsure", "Garment Sleeve": "long sleeves", "Garment Pocket": "pocket", "Garment Collar": "collar"} is formulated into "A person wearing long-sleeved collared red upper garment with pockets".
- **Fine-Grained Subdataset:** Unlike the Mixed-Grained Subdataset, where feature selection is random, all eight features are un.masks for this subdataset. To evaluate the model’s sensitivity to fine-grained details, each trap is designed such that the **Garment Type** and **Garment Color** are always identical to those of a target in the same video. Consequently, the traps and targets differ only in the finer-grained features. *Example:* {"Garment Color": "white and brown", "Garment Shade": "light", "Glasses": "no glasses", "Garment Type": "jacket", "Garment Sleeve": "long sleeves", "Garment Pocket": "no pocket", "Garment Collar": "collar", "Gender": "male"} is equal to "A man wearing light long-sleeved collared red jacket with pockets and not wearing glasses".

B.4 Stage hallucination

B.4.1 Uniqueness of Stage. As discussed in A, videos rely on multi-frame sequences to convey chronological information, with actions across frames serving as key content. A video may include multiple characters performing similar actions, requiring humans to first identify the subject to understand the action. For example, in Figure 2, the actions "a man in a blue jacket walks into the room and closes the door" and "a woman in a beige jacket leaves the hallway" illustrate distinct interactions involving characters, actions, and objects—critical for video understanding. Dialogue is treated as a unique action set, as recognizing the speaker is essential for understanding video content, especially when combined with facial expressions and audio. For instance, in Figure 2, the video features four main characters, each delivering a passage in specific clips. Identifying the speaker requires linking their dialogue to their features during these moments.

B.4.2 Filtering dialogue details. To reduce time and cost, we utilize existing question-answer pairs from the TVQA+ dataset, denoted as $QA = \{q, [c_1, c_2, c_3, c_4, c_5], a\}$, to construct the event hallucination benchmark. However, two challenges arise in reusing this data. First, the characters in QA are typically referred to by name (e.g., “Sheldon”, “Leonard”, “Penny”), which is unsuitable for a general-purpose video understanding benchmark. Using the person feature annotations introduced in the previous section, we replace names with coarse-grained descriptions (e.g., “a man wearing a blue T-shirt”). Second, some QA pairs rely on subtitle-based information. To ensure the remaining QA require only visual understanding, we design Algorithm 4, which filters out questions containing n-grams that appear solely in the subtitle sequence $S_{Sub} = [Sub_1, Sub_2, \dots, Sub_n]$ but not in the object set S_o . The algorithm outputs Stm , a description of a single event in the video. If the corresponding flag $B = \text{False}$, the Stm is retained and used as the target event for generating event hallucination questions. Detailed process is listed in Algorithm 4.

Algorithm 4 Subtitle Filter

Input: TVQA+ Question answer pair $QA = (q, [c_1, c_2, c_3, c_4, c_5], a)$, Subtitles list $S_{Sub} = [Sub_1, Sub_2, \dots, Sub_n]$, Object set $S_o = \{o_1, o_2, \dots, o_m\}$.

```

1:  $Stm \leftarrow \text{LLM}(\text{"... Convert the question answer pair } \{q, c_a\} \text{ into several declarative sentences ..."} )$ 
2:  $Stm_{norm} \leftarrow \text{LLM}(\text{"... Extract all the norms that appear in } Stm \text{ ..."} )$ 
3:  $Sub_{norm} \leftarrow \text{LLM}(\text{"... Extract all the norms that appear in } S_{Sub} \text{ ..."} )$ 
4:  $B \leftarrow \text{False}$ 
5: for  $norm_i$  in  $Stm_{norm} = \{norm_1, norm_2, \dots, norm_\alpha\}$  do
6:   if  $norm_i \in Sub_{norm}$  and  $norm_i \notin S_o$  then
7:      $B \leftarrow \text{True}$ 
8:     break
9:   end if
10: end for
Output:  $Stm$  that describe part of the video, Whether the statement involved content from subtitle  $B$ .
```

B.4.3 Annotated dialogues. Conversation extraction is performed by analyzing TVQA+ subtitle talking information to identify conversational exchanges. Initially, the speaker’s identity and temporal metadata (start/end timestamps) are extracted from the raw subtitle material. Subsequently, speaker names are systematically substituted with their corresponding feature descriptors (e.g., “woman in a red blouse”, “man with glasses”) using a predefined feature database derived from the person feature dataset. This process ensures anonymization while preserving contextual relevance through attribute-based identification. As illustrated in Figure 5a, this method produces anonymous output, such as “A woman in a red dress without glasses is talking”, showing how the conversation is extracted from the video clip.

B.4.4 Annotated actions. The retain Stm from Algorithm 4 are then parsed to extract actions in the syntactic template “subject-action”, where subject represents the agent and “action” represent the action performed by the agent (e.g., drinking white wine, sitting at the table eating dinner, or running into the door). Names within these extracted actions are substituted with their corresponding feature descriptors (e.g., garment type, gender) derived from the pre-extracted person feature database. The target is assembled by the feature descriptors and corresponding action. For the traps, to generate different categories of traps, a pool of subject and action is collected and different selecting algorithm is applied in Algorithm 5, which is discussed in detailed in the next section B.4.5.

B.4.5 Selecting Stage. For the selection stage in the dialogue dataset, two distinct motion hallucination categories are formally defined by replacing the original speaker with different types of individuals. The details of these categories are explained below, with the video clip from Figure 5a serving as an example:

- **Character out of Video (CO):** Generated by substituting the speaker with a non-existent person in the video. *Example:* From “A woman in a red dress without glasses is talking” to “A man in a red jacket without glasses is talking”, where “A man in a red jacket without glasses” has never appeared in the entire video.
- **Character in Video (CI):** Generated by replacing the speaker with a person present in the video clip who has never spoken throughout the video. *Example:* From “A woman in a red dress without glasses is talking” to “A man in a black suit with glasses is talking”, where “A man in a black suit with glasses” exists in the video but has never spoken.

For the selecting stage in the non-dialogue dataset, by synthesizing agents and their corresponding actions from heterogeneous sources, five distinct motion hallucination categories are formally defined. Details of the five types are explained below, with the video clip from Figure 5b serving as an example:

- **Action out of Video (AO):** Constructed by pairing individuals present in the video with actions derived from external video contexts. *Example:* From “A man in a blue jacket without glasses is walking into the room” to “A man in a blue jacket without glasses is cooking some food”, where “cooking some food” is an action from other video clips.

Algorithm 5 Action Hallucination Questions Construction

Input: Video-Statement dictionary $\mathbb{D} = \{v_1 : [Stm_1^{v_1}, Stm_2^{v_1}, \dots], v_2 : [\dots], \dots\}$, Random sample algorithm $Random_c$, Number of Iteration n_t .

```

1:  $\mathbb{S}_A \leftarrow \{\}$ .
2:  $\mathbb{S}_P \leftarrow \{\}$ .
3: for  $Stm_j^{v_i}$  in  $\mathbb{D}$  do
4:    $(P, A) \leftarrow \text{LLM}(\text{"... divide the statement } Stm_j^{v_i} \text{ into two parts: subjective and action ..."}).$ 
5:    $\mathbb{S}_A \leftarrow \mathbb{S}_A \cup \{A\}$ .
6:    $\mathbb{S}_P \leftarrow \mathbb{S}_P \cup \{P\}$ .
7: end for
8:  $\mathbb{D}_{trap} \leftarrow \{\}$ .
9: for  $v_i$  in  $\mathbb{D}$  do
10:   $\mathbb{D}_{trap} \leftarrow \mathbb{D}_{trap} \cup \{v_i : \{\}\}$ 
11:  for iteration = 1, 2, ...,  $n_t$  do                                ▶ Loop 1
12:     $A_{trap} \leftarrow Random_c(\mathbb{S}_A)$ .
13:     $P_{trap} \leftarrow Random_c(\mathbb{S}_P)$ 
14:     $Stm_{trap} \leftarrow P_{trap} + A_{trap}$ 
15:    for  $Stm_j^{v_i}$  in  $\mathbb{D}[v_i]$  do
16:      if  $Stm_{trap} \approx Stm_j^{v_i}$  then
17:        break Loop 1.
18:      end if
19:    end for
20:     $\mathbb{D}_{trap}[v_i] \leftarrow \mathbb{D}_{trap}[v_i] \cup \{Stm_{trap}\}$ 
21:  end for
22: end for
Output: Trap dictionary  $\mathbb{D}_{trap}$ .

```

- **Character out of Video (CO):** Generated by integrating extraneous agents (not present in the video) with actions native to the original scene. *Example:* From “A man in a blue jacket without glasses is walking into the room” to “A woman in a blue jacket without glasses is walking into the room”, where “A woman in a blue jacket without glasses” has never appeared in the video.
- **Similar Action (SA):** Created by semantically perturbing in-scene actions to produce plausible yet absent variants. *Example:* From “A man in a blue jacket without glasses is walking into the room” to “A man in a blue jacket without glasses is jumping outside the room”, where “jumping outside the room” is a semantically related yet non-occurring action.
- **Mixed in Video (MI):** Formulated by interchanging roles between existing agents and their associated actions. *Example:* Swapping descriptors such as “A man in a blue jacket without glasses is walking into the room” and “A man in a gray t-shirt is sitting” to generate “A man in a blue jacket without glasses is sitting” and “A man in a blue jacket without glasses is sitting”, where the two actions before the change are actions that exist in the video clip.

B.4.6 Quality Guarantee. Finally, to guarantee traps can be clearly distinguished from the target instead of simply “rephrasing” the description, *text-embedding-3-small*¹ is utilized to vectorized the targets and the trap. If the similarity between targets and the trap, which is calculated by Cosine Distance, is greater than 0.65, then the trap will be abandoned. This mechanism is represented by operation “ \approx ” in Algorithm 5. The formal construction process is listed in Algorithm 5.

B.5 Spatial-Temporal Hallucination

After aligning characters with their movements, humans naturally interpret multiple actions by noticing and using their temporal order. Extending our hallucination benchmark to a higher level, we therefore evaluate the model’s understanding of temporal order. Using the existing question–answer pairs and time-slot annotations from the TVQA+ dataset, we construct a small dataset specifically for evaluating temporal hallucination. As with stage annotation pipeline in B.4.2, QA pairs that rely only on subtitle-based information are filtered out, and the remaining pairs are transformed into *Stm*. Consequently, for each video, we obtain a list of actions along with their corresponding start and end timestamp tuples.

$$[(Stm_1, ts_1^s, ts_1^e), \dots, (Stm_i, ts_i^s, ts_i^e), \dots, (Stm_n, ts_n^s, ts_n^e)]$$

We select suitable videos and their corresponding action lists using the following criterion:

¹<https://platform.openai.com/docs/guides/embeddings>

$$\exists i, j, k \in \{1, \dots, n\} \text{ and } i \neq j \neq k \text{ such that } ts_i^e < ts_j^i \text{ and } ts_j^e < ts_k^s$$

This ensures that there are at least three distinct actions occurring in a strict temporal order. The selected actions are then randomly permuted to create a spatial-temporal hallucination question. An example is shown in Figure 13. In the experiments, we uniformly sample 64 frames from each video and provide them to the LVM along with the constructed question. The results are reported in Table 9.

Example Question of Temporal Hallucination	
Question:	
There are three events happening in the video:	
1. A man wearing a blue t-shirt holds up a fork.	
2. A woman wearing a yellow dress puts her hand in her purse.	
3. A woman wearing a yellow dress knocks on the door.	
You need to find correct order of these events among the following options. Options:	
A. Event 1 happens first, followed by Event 2, and finally Event 3.	
B. Event 3 happens first, followed by Event 1, and finally Event 2.	
C. Event 2 happens first, followed by Event 3, and finally Event 1.	
D. Event 1 happens first, followed by Event 3, and finally Event 2.	
Please select the correct answer (A/B/C/D):	

Figure 13: An example of spatial-temporal hallucination question. The 1, 2, and 3 in the question can be permuted or substituted with different event description.

Table 9: Temporal hallucination experiment results on a small set of models.

Model	LLaVA-Video-7B	LLaVA-OV-7B	Qwen2-VL-7B	Qwen2-VL-2B	InternVL2.5-8B	InternVL2.5-2B
Performance	0.515	0.431	0.389	0.198	0.393	0.290

The results are broadly consistent with before. This suggests that higher-level interpretations rely on the correctness of lower-level hallucinations, supporting our bottom-up framework design. Notably, the *LLaVA-Video* model, finetuned on video data, outperforms both the *LLaVA-OV* model and other models. Furthermore, the complexity of temporal relations, long input sequences, and rich action contexts make temporal hallucination particularly challenging for LVMs.

B.6 Generalization of MESH Pipeline



Figure 14: Using YOLO to generate bounding boxes for the characters in UCF101 dataset

The setting–character–stage framework is widely used to analyze complex videos like films and TV series, which offer richer information flow than everyday footage. We chose TVQA+ for its dense annotations and rich visual cues—e.g., camera movement and character actions (see Figure 2). Rose [64] shows this approach generalizes to other video types. We demonstrate how our categorization and annotation pipeline can be applied across datasets.

- **Setting: environments and objects** Location labels (e.g., “living room,” “kitchen”) are accurately generated using GPT-4o. While object annotations in TVQA+ are sparse, they can be supplemented using human labelers or vision models. Like humans, these models may miss some objects but can reliably infer environment contexts.
- **Characters: features and identity** Most video datasets lack fine-grained human annotations, which we address with a **bounding-box-first** pipeline. Using YOLO [63] (see Figure 14) to generate bounding boxes, we annotate physical features verified by human labelers. Such verification process is also seen in other datasets [19, 67]. This supports precise character recognition and enables generation of hallucination and stage questions based on diverse character–action pairs.
- **Stage: leveraging action annotations** Many datasets already include useful action labels [17, 69], which we pair with character features to generate stage-related questions. Dialogue attribution is straightforward via subtitles or audio and typically requires no manual annotation.

To further verify the generalization ability of MESH category and pipeline, we apply them to the UCF101[70] dataset. As mentioned above, for the setting hallucination, we prompt GPT-4o to generate the locations and objects appear in the video. Then, human annotator will examine the correctness of generated labels. Finally, the location and object labels are feed into the same pipeline described in B.2 to generate targets and traps. The experiments result on UCF101 setting hallucination is presented in Table 10.

Table 10: Setting hallucination on UCF101

Model	LLaVA-Video-7B	LLaVA-OV-7B	Qwen2-VL-7B	Qwen2-VL-2B	InternVL2.5-8B	InternVL2.5-2B
Binary Task	0.945	0.930	0.956	0.937	0.894	0.868
Multi-Choice Task	0.978	0.919	0.905	0.992	0.926	0.905

For the character hallucination, after generating bounding box for the people that appear in the video, the bounding box and video are feed into MESH character hallucination pipeline B.3 to generate questions. The result is presented in Table 11.

Table 11: Character hallucination on UCF101

Model	Grain	Binary Task			Multi-Choice Task		
		Short	Medium	Long	Short	Medium	Long
LLaVA-Video-7B	Coarse	0.964	0.956	0.964	0.964	0.964	0.964
	Medium	0.894	0.894	0.912	0.824	0.842	0.859
	Mixed	0.842	0.780	0.807	0.771	0.807	0.807
	Fine	0.771	0.789	0.780	0.754	0.701	0.719
LLaVA-OV-7B	Coarse	0.964	0.938	0.912	0.964	0.912	0.929
	Medium	0.859	0.850	0.833	0.771	0.789	0.824
	Mixed	0.789	0.780	0.780	0.736	0.807	0.789
	Fine	0.719	0.719	0.710	0.596	0.596	0.614

Preliminary results reveal both similarities and differences between the TVQA+ and UCF101 datasets. First, UCF101 is simpler, with short (~10s) videos and fixed locations. Second, in both benchmarks, character hallucination follows the same trend: finer granularity leads to lower accuracy. Third, TVQA+ shows a negative correlation between the number of input frames and accuracy, whereas UCF101 does not, likely due to its simplicity—more frames do not add useful information. Finally, unlike TVQA+, each UCF101 video contains only one character and one action, making it insufficient for stage hallucination evaluation.

To address this, we construct the UCF101-COMBINE dataset by concatenating 4–5 UCF101 videos into one, better matching the complexity of TVQA+. We then apply the setting and character hallucination pipelines, with results reported in Table 12 and Table 13.

Table 12: Setting hallucination on UCF101-COMBINE

Model	LLaVA-Video-7B	LLaVA-OV-7B	Qwen2-VL-7B	Qwen2-VL-2B	InternVL2.5-8B	InternVL2.5-2B
Binary Task	0.926	0.899	0.864	0.732	0.768	0.705
Multi-Choice Task	0.969	0.911	0.854	0.872	0.896	0.778

Table 13: Character hallucination on UCF101-COMBINE

Model	Grain	Binary Task			Multi-Choice Task		
		Short	Medium	Long	Short	Medium	Long
LLaVA-Video-7B	Coarse	0.928	0.892	0.852	0.941	0.868	0.838
	Medium	0.884	0.827	0.776	0.827	0.775	0.737
	Mixed	0.850	0.817	0.769	0.788	0.713	0.620
	Fine	0.855	0.807	0.724	0.721	0.635	0.581
LLaVA-OV-7B	Coarse	0.912	0.860	0.816	0.920	0.866	0.769
	Medium	0.845	0.785	0.724	0.730	0.642	0.558
	Mixed	0.838	0.743	0.675	0.709	0.601	0.517
	Fine	0.822	0.728	0.633	0.532	0.480	0.407
Qwen2VL-7B	Coarse	0.880	0.816	0.789	0.875	0.782	0.689
	Medium	0.794	0.757	0.667	0.655	0.575	0.504
	Mixed	0.797	0.721	0.695	0.633	0.562	0.461
	Fine	0.812	0.711	0.614	0.495	0.435	0.381
Qwen2VL-2B	Coarse	0.846	0.775	0.700	0.859	0.773	0.674
	Medium	0.699	0.587	0.552	0.642	0.592	0.510
	Mixed	0.732	0.643	0.571	0.536	0.448	0.385
	Fine	0.735	0.609	0.549	0.525	0.467	0.411
InternVL2.5-8B	Coarse	0.858	0.789	0.743	0.884	0.855	0.802
	Medium	0.764	0.741	0.681	0.762	0.728	0.636
	Mixed	0.717	0.695	0.621	0.679	0.604	0.536
	Fine	0.721	0.667	0.604	0.621	0.565	0.472
InternVL2.5-2B	Coarse	0.917	0.869	0.806	0.935	0.887	0.825
	Medium	0.859	0.774	0.681	0.795	0.728	0.659
	Mixed	0.764	0.689	0.606	0.668	0.590	0.461
	Fine	0.766	0.684	0.551	0.579	0.525	0.467

Results on the UCF101-COMBINE dataset are more consistent with those on TVQA+. Since each combined video includes multiple characters and actions, we can apply the stage hallucination pipeline (Section B.4). The results are given in Table 14.

Table 14: Stage hallucination on UCF101-COMBINE

Category	LLaVA-Video-7B	LLaVA-OV-7B	Qwen2-VL-7B	Qwen2-VL-2B	InternVL2.5-8B	InternVL2.5-2B
AOV	0.955	0.917	0.860	0.799	0.890	0.856
COV	0.766	0.671	0.637	0.471	0.636	0.622
MIV	0.606	0.474	0.476	0.295	0.543	0.451

Overall, applying the MESH categories and pipeline to the UCF101-COMBINE dataset replicates the key phenomena observed on TVQA+, demonstrating both the generalization of the MESH pipeline and the universality of our conclusions. At the same time, minor differences emerge. For instance, while the original UCF101 shows no correlation between video length and accuracy, in UCF101-COMBINE the accuracy on the COV stage hallucination category is consistently lower than on AOV. A likely reason is that actions are more salient, leading models to rely on them while ignoring character features. These subtle differences highlight that applying the MESH pipeline to new datasets can yield novel insights into LVMS’ understanding of different videos types.

C Experiments

C.1 General details

C.1.1 Difficulty level. For **setting**, all questions are classified as **basic**. For **characters**, questions on **coarse** and **medium**-level features are **basic**, while **mixed** and **fine**-level features are **advanced**. For **stage**, all **binary** questions are **basic**. For **action MC questions**, AO and CO are **basic**, while SA and MI are **advanced**. For **dialogue MC questions**, CO is **basic**, and CI is **advanced**.

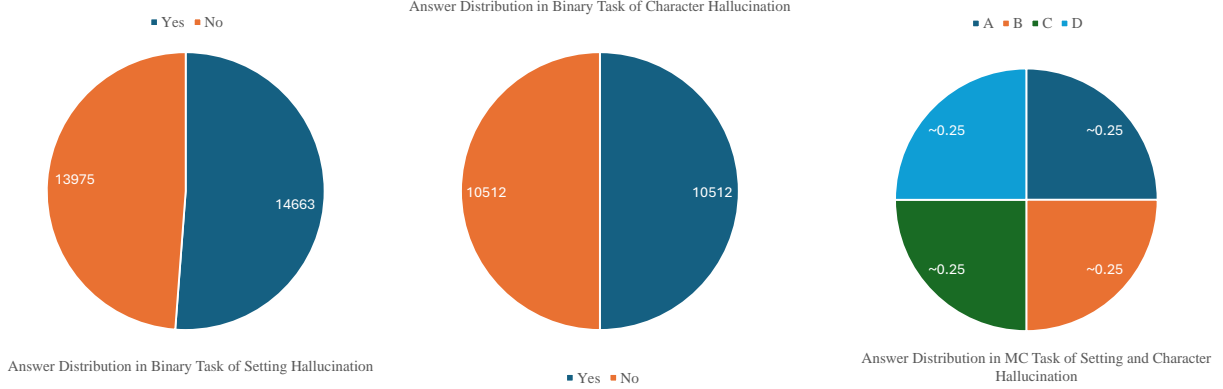


Figure 15: Answer Distribution for binary task and multi-choice task in Setting and Character Hallucination.

C.1.2 Dataset Statistics. The datasets employed in this study—the **Setting Hallucination Dataset** and the **Character Hallucination Dataset**—are structured into binary classification and multiple-choice task formats. Across these datasets and their associated subdatasets (detailed in Section B.3.2), the binary classification tasks maintain a balanced class distribution. In contrast, the multiple-choice tasks comprise questions with four answer options, each displaying an approximately uniform empirical distribution across all evaluated subdatasets, as illustrated in Figure 15.

The **Stage Hallucination Dataset** is similarly organized into binary classification and multiple-choice tasks but is further divided into two types and four distinct categories based on its generation methods (see Section B.4.5 for details). Unlike the Setting and Character Hallucination datasets, the Stage Hallucination Dataset exhibits distinct distribution patterns across its categories and answer options. These differences are visually represented in Figures 16 (action) and 17 (dialogue), highlighting its unique structural and characteristics.

Stage Hallucination Dataset (Action).

- **Binary Classification Task:** (Figure 16 left) The dataset includes 17,577 questions (2,488 labeled "yes" and 15,089 labeled "no"). The "no" responses are categorized into four groups: "AO" (6,518), "CO" (7,131), "SA" (1,200), and "MI" (240).
- **Multi-Choice Task:** (Figure 16 right) This task consists of a total of 12,021 questions. Those questions are divided into four partitions: "AO"(3,597), "CO" (4,637), "SA" (3,507), "MI"(280).

Stage Hallucination Dataset (Dialogue).

- **Binary Classification Task:**(Figure 17 left) This subset contains 16,155 questions (2,303 labeled "yes" and 13,852 labeled "no"). The "no" answers are classified into three categories: "AO" (5,646), "CO" (6,756), and "CI" (1,450).
- **Multi-Choice Task:**(Figure 17 right) There are a total of 4,654 questions in this category. The category distributions are as follows: "CO" (2,327), "CI" (2,327).

C.1.3 Evaluated Video-Language Models. This section introduces the video-language models (LVLMs) evaluated in this study, providing a rationale for their selection and a concise overview of their key architectural characteristics. The models selected represent a range of design choices and technological advancements within the field, allowing for a comprehensive analysis of performance across diverse benchmarks. We highlight variations in Large Language Model (LLM) backbones and vision encoders, as well as innovative techniques employed for video understanding and efficient processing.

- **Video-LLaVA** [43]: This model leverages the Vicuna [14] LLM and the languageBind [26] vision encoder. LanguageBind is pre-trained on a diverse set of modalities, including video, audio, infrared, and depth data, enabling enhanced video understanding capabilities. The selection of languageBind as a vision encoder aims to evaluate the influence of diverse pre-training modalities on video-language understanding.
- **LLaVA-NeXT-Video** [85]: This model exhibits a scale-dependent architectural design. The 7B parameter version integrates Vicuna [14] with the CLIP [62] vision encoder, while the 32B parameter version employs Qwen1.5 [3] as the LLM and SigLIP as the vision

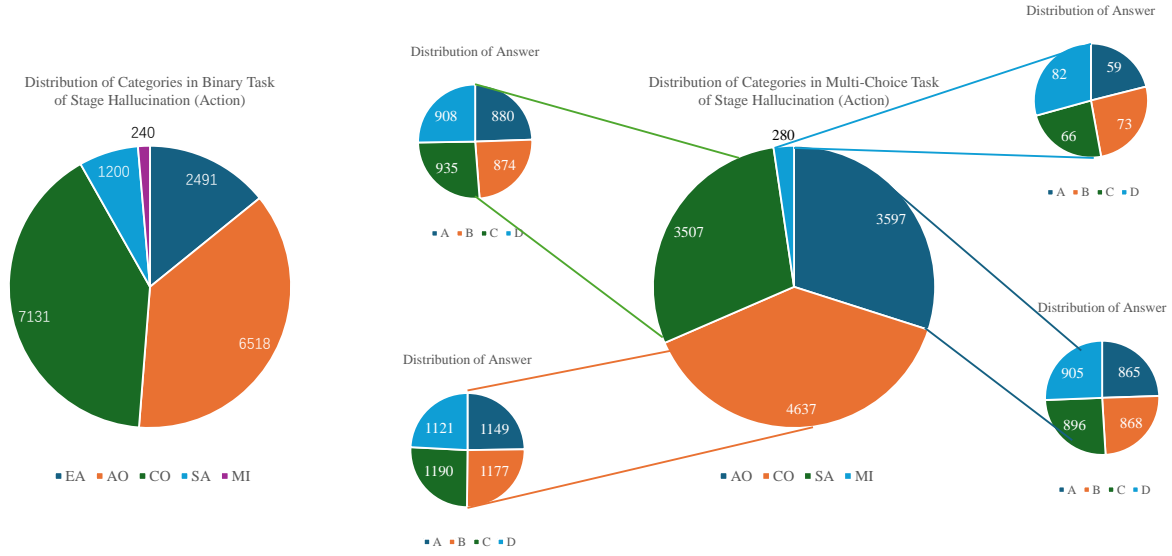


Figure 16: Category and answer distribution for binary task and multi-choice task in Stage Hallucination (Action).

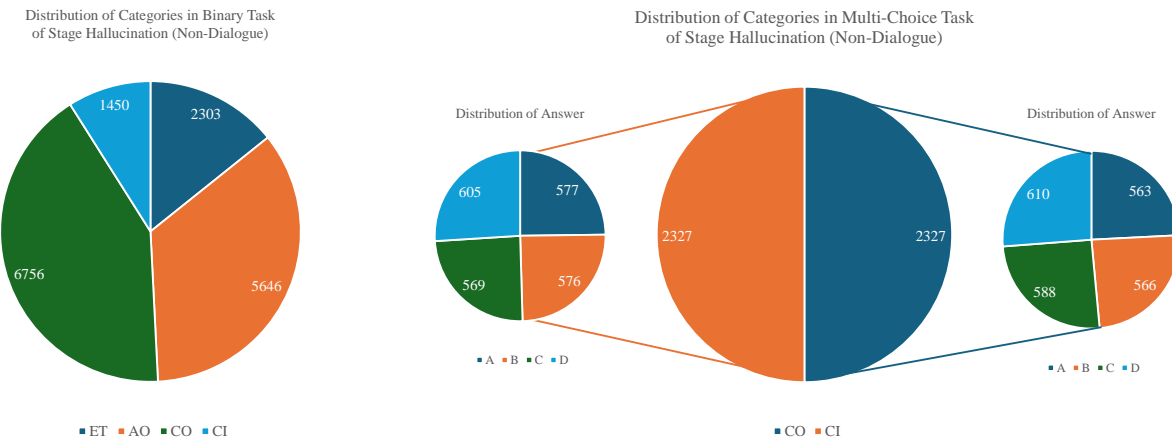


Figure 17: Category and answer distribution for binary task and multi-choice task in Stage Hallucination (Dialogue).

encoder. The inclusion of LLaVA-NeXT-Video allows for investigation of the interplay between LLM scale, vision encoder choice, and resulting performance.

- **LLaVA-Video** [86]: This LVLM utilizes the Qwen2 [77] LLM, known for its strong performance on language tasks, and the SigLIP vision encoder, which has demonstrated competitive results in various vision-related benchmarks. Comparing with previous model can provide more in-depth analysis on different LLMs and vision encoders.
- **LLaVA-OneVision** [36]: Leveraging the Qwen2 LLM and SigLIP vision encoder, this model is designed to excel in understanding single images, multiple images, and video data. Its selection allows for a performance comparison between video models and general purpose models.

- **Aria** [38]: This model uses SigLIP as the vision encoder and a Mixture of Experts (MoE) architecture LLM with a total of 23B parameters. During token prediction, only 3.9B parameters are activated. This design choice allows for experimentation with parameter efficient LLMs.
- **LLaMA-VID** [42]: Employing the CLIP vision encoder and Vicuna as the LLM, LLaMA-VID incorporates a novel multi-modal adapter. This adapter reduces the number of image tokens to two per image, enabling efficient inference on long video sequences. Its inclusion tests the impact of adapter on tokens and inference.
- **Oryx** [51]: Utilizing the Qwen2 LLM and SigLIP as the vision encoder, Oryx introduces a dynamic downsampling layer tailored for video processing. This layer comprises a 4x4 pooling layer and a regional cross-attention layer. The inclusion of Oryx assesses the impact of different video processing techniques.
- **Qwen2VL** [77]: This model uses Qwen2 as its LLM and features a specialized vision encoder capable of encoding video frames into a variable number of tokens, adaptable to different specifications and resolutions.
- **VideoAgent** [22]: This model adopts an agent-based approach, employing an LLM as the agent and utilizing diverse vision foundation models as tools. Function calling via LangChain² is used to leverage these tools for completing video understanding tasks. This choice allows for evaluation of the agent-based approach.
- **VILA** [44]: Integrating the LLaMA3 [75] as LLM, VILA incorporates image-text interleaved training. This approach is reported to yield significant performance gains in image, multi-image, and video understanding tasks.
- **InternVL2.5** [11]: This model uses InternLM [9] as its LLM and InternViT [12] as its vision encoder, where the latter is jointly trained with the LLM using various objective functions. Its training data underwent careful filtering and augmentation.
- **VideoXL** [68]: VideoXL leverages SigLIP as the vision encoder and Qwen2 as the LLM. It is enhanced by a visual token compression module that groups similar tokens into visual summary tokens. This compression mechanism facilitates the handling of thousands of video frames during training and inference.
- **VideoLLaMA2** [13]: This model employs SigLIP and Qwen2, and implements a novel Spatial-Temporal Convolution Connector which consists of RegStage and 3D convolution layers to help spatial and temporal information aggregation for the process of vision feature extraction in videos.
- **Claude 3.5-Sonnet** [2]: A proprietary video-language model developed by Anthropic. Its inclusion allows comparison of opensource model with one of the popular closesource models.
- **GPT-4o** [30]: A proprietary video-language model developed by OpenAI. Comparing with other models enables in-depth research.
- **Gemini 1.5-Pro** [73]: A proprietary video-language model developed by Google. This allows assessment by one of the most popular model in the field.

C.1.4 Technique Details.

Deployment of Larger LVLMs with 8×A800 GPUs. For LVLMs exceeding 70 billion parameters—such as LLaVA-Video-72B, InternVL2.5-78B, Qwen2VL-72B, and LLaVA-OneVision-72B—we employ a high-performance computing node equipped with 8 NVIDIA A800 GPUs. To optimize inference speed, different deployment frameworks are utilized based on official recommendations and support. Specifically, LLaVA-OneVision-72B and Qwen2VL-72B, which provide official support for vLLM [34], are deployed and evaluated using this framework. InternVL2.5-78B is deployed using the lmdeploy [18] framework, as recommended by its developers. For LLaVA-Video-72B, since it has not yet been integrated into other frameworks, we utilize the Hugging Face Transformers library [79] for deployment and evaluation.

Deployment of Smaller LVLMs with RTX 3090/4090 GPUs. For LVLMs with fewer than 40 billion parameters—such as VILA1.5-8B, Aria-23B, and LLaVA-NeXT-Video-32B—the Hugging Face Transformers library is employed for model deployment and experimentation. To minimize computational costs, these models are deployed on consumer-grade GPUs, specifically the NVIDIA RTX 3090 and RTX 4090.

C.2 Setting hallucination

We present the detailed experiment settings and results in Table 18. Experiments on closed-source general models are given in Table 15. Compared to open-source LVLMs, these models show no significant overall performance improvement. Furthermore, on the MC task, all models underperform compared to the state-of-the-art LLM. This suggests that while popular multi-modality API-based models excel at object-scene distinction, they struggle in scenarios with increased confounding objects.

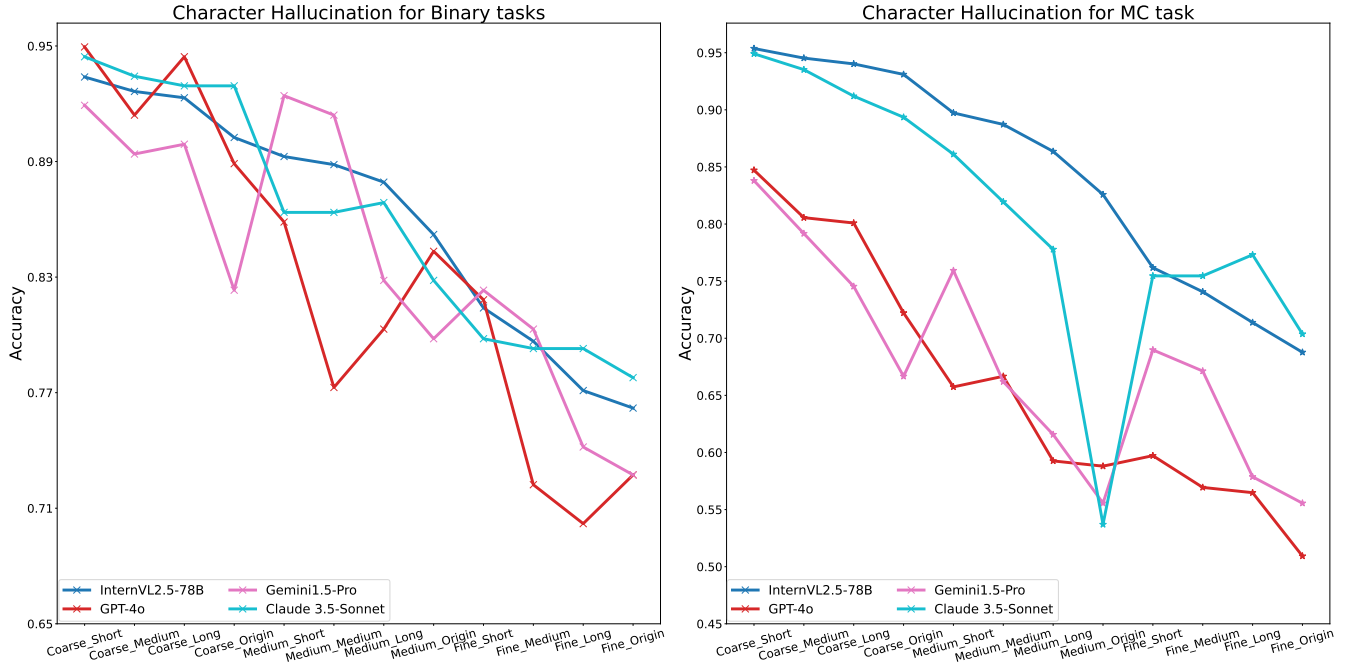
²<https://www.langchain.com/>

Table 15: Close-source models on Setting for Binary/MC tasks.

Model	Binary (%)		MC (%)		
	Acc	Pos	Acc	OB	COB
Best LVM	90.3	49.1	94.9	0.71	0.52
GPT-4o	92.6	50.4	86.6	2.65	2.30
Gemini1.5-Pro	90.6	49.8	83.8	3.38	2.29
Claude 3.5-Sonnet	90.0	44.5	85.8	2.16	2.37

C.3 Character hallucination

We present the detailed experiment settings and results in Table 19 and 20. For closed-source general models, Figure 18 presents the comparison. These models generally follow the same decreasing trend as LVMs, from coarse to fine features and short to long video lengths. On binary tasks, their performance is comparable to the best LVM, but on the MC task, most underperform relative to InternVL2.5-78B, consistent with the results in Setting. A notable difference is their greater instability when varying feature granularity and video length, highlighting the challenges of using general models for video inputs.

**Figure 18: Close-source models on Character for Binary/MC tasks.**

C.4 Stage hallucination

We present the detailed experiment settings and results for action part in Table 21 and 22. We present the detailed experiment settings and results for dialogue part in Table 24 and 23. The comparison in Tables 16 and 17 shows that closed-source general models perform significantly worse than state-of-the-art LVMs. This is because specialized LVMs are fine-tuned on video datasets for video understanding. These results confirm our assumption that stage questions rely heavily on chronological information, requiring LVMs to leverage multi-frame data effectively—a capability general models lack.

Table 16: Close-source models on Stage: Action

Model	Binary %		MC %	
	Acc	JSD	Acc	JSD
Best LVM	85.3	0.05	85.5	0.05
GPT-4o	81.4	0.15	67.3	0.66
Gemini1.5-Pro	73.3	0.03	60.6	0.22
Claude 3.5-Sonnet	73.0	0.03	75.1	0.52

Table 17: Close-source models on Stage: Dialogue

Model	Binary %		MC %	
	Acc	JSD	Acc	JSD
Best LVM	80.6	4.40	83.8	0.09
GPT-4o	79.3	0.14	73.4	0.45
Gemini1.5-Pro	82.3	0.77	77.9	0.33
Claude 3.5-Sonnet	78.1	0.02	77.8	0.34

D Additional Tables

Table 18: Detailed performances on Setting for Binary/MC tasks.

Model	NSF	LLM	Binary Task			Multi-Choice Task			
			Acc.	Pos.	JSD.	Acc.	OB.	COB.	JSD.
GPT-4o	32	GPT-4o	.9261	.5041	.000228	.8659	.02650	.02303	.001246
Gemini1.5-Pro	32	Gemini1.5-Pro	.9064	.4975	.000390	.8379	.03376	.02292	.002049
Claude 3.5-Sonnet	32	Claude 3.5-Sonnet	.8998	.4450	.003243	.8577	.02156	.02373	.000344
LLaVA-Video-7B	32	Qwen2	.9064	.4948	.000148	.9211	.00377	.00152	.000085
LLaVA-Video-72B	32	Qwen2	.9032	.4905	.000297	.9225	.00757	.00645	.000037
Aria-23B	32	Aria	.9003	.4335	.003091	.8564	.01950	.00796	.001334
VILA1.5-8B	32	Llama3	.8724	.4809	.000488	.7616	.01577	.00566	.000869
InternVL2.5-78B	32	Qwen2.5	.8692	.4011	.006598	.9486	.00710	.00524	.000095
Qwen2VL-7B	32	Qwen2	.8585	.3971	.006669	.7319	.02753	.01995	.002237
LLaVA-OneVision-72B	32	Qwen2	.8384	.5141	.000000	.8296	.03133	.01609	.002189
LLaVA-OneVision-7B	32	Qwen2	.8325	.5427	.000474	.8413	.04991	.02178	.006868
LLaVA-OneVision-7B-chat	32	Qwen2	.8303	.5559	.000977	.8408	.04799	.02126	.006395
VideoLLaMA2.1-7B	32	Qwen2	.8258	.3614	.011579	.8493	.02505	.01206	.001684
LongVILA-8B	32	Llama3	.8070	.6590	.011117	.6633	.13745	.08129	.056180
LLaMA-VID-13B	32	Vicuna	.8010	.6557	.010416	.5416	.19723	.09765	.089951
InternVL2.5-4B	32	Qwen2.5	.7941	.4835	.000408	.8194	.02835	.01002	.002259
Qwen2VL-72B	32	Qwen2	.7841	.3140	.020958	.8634	.01520	.00897	.000840
InternVL2.5-8B	32	InternLM2.5	.7837	.4618	.001251	.8236	.00782	.00441	.000317
InternVL2.5-2B	32	InternLM2.5	.7803	.4134	.004898	.7577	.04353	.01693	.005349
VideoXL-7B	32	Qwen2	.7709	.5016	.000072	.7295	.00927	.00666	.000249
Qwen2VL-2B	32	Qwen2	.7694	.2969	.024246	.8124	.04746	.03029	.007235
LLaVA-NeXT-Video-7B	24	Vicuna	.7608	.2827	.028414	.8190	.05766	.02434	.007810
VideoAgent	ALL	Agent	.7236	.5097	.000019	.6669	.03081	.02114	.002765
InternVL2.5-1B	32	Qwen2.5	.6815	.5662	.001477	.5414	.02313	.01759	.001265
Oryx1.5-7B	32	Qwen2.5	.6935	.2627	.033192	.6621	.03468	.01809	.003739
Oryx1.5-32B	32	Qwen2.5	.6896	.2328	.043309	.6278	.05836	.02704	.011931
Oryx-7B	32	Qwen2	.6836	.2242	.045420	.6256	.03264	.01731	.002877
LLaVA-NeXT-Video-32B	32	Qwen1.5	.6298	.8634	.074071	.8137	.02781	.01349	.001802
LLaMA-VID-7B	32	Vicuna	.5504	.9260	.114913	.4847	.20300	.10089	.095066
Video-LLaVA-7B	32	Vicuna	.5211	.9888	.184722	.3306	.35279	.27039	.299236
LLaVA-OneVision-0.5B	32	Qwen2	.5121	.9998	.208337	.6490	.13945	.06964	.050139
LLaMA-VID-Long-Video	32	Vicuna	.4725	.3077	.021879	.2346	.36924	.37310	.339778

NSF for number of sampling frames. LLM for language backbones. OB and COB denote object-related metrics in multi-choice evaluation.

Table 19: Accuracy performances on Character Hallucination

Model	Grain	Binary Task				Multi-Choice Task			
		Short	Medium	Long	Origin	Short	Medium	Long	Origin
GPT-4o	Coarse	.9495	.9141	.9444	.8889	.8472	.8056	.8009	.7222
	Medium	.8586	.7727	.8030	.8434	.6574	.6667	.5926	.5880
	Mixed	.7879	.7576	.7273	.7525	.6204	.5741	.5417	.5139
	Fine	.8182	.7222	.7020	.7273	.5972	.5694	.5648	.5093
Gemini1.5-Pro	Coarse	.9192	.8939	.8990	.8232	.8380	.7917	.7454	.6667
	Medium	.9242	.9141	.8283	.7980	.7593	.6620	.6157	.5556
	Mixed	.8030	.7929	.7525	.7424	.6481	.5972	.5163	.5278
	Fine	.8232	.8030	.7418	.7273	.6898	.6713	.5787	.5556
Claude 3.5-Sonnet	Coarse	.9444	.9343	.9293	.9293	.9491	.9352	.9120	.8935
	Medium	.8636	.8636	.8687	.8283	.8611	.8194	.7778	.5370
	Mixed	.7980	.8384	.8081	.7828	.7361	.7222	.7037	.6806
	Fine	.7980	.7929	.7929	.7778	.7546	.7546	.7731	.7037
LLaVA-Video-7B	Coarse	0.9299	0.9217	0.9102	0.8872	0.9491	0.9389	0.9268	0.905
	Medium	0.8139	0.7997	0.7792	0.732	0.7972	0.7724	0.744	0.6779
	Mixed	0.7637	0.7483	0.7304	0.6882	0.6638	0.6419	0.6148	0.5551
	Fine	0.7451	0.7251	0.6998	0.6511	0.5802	0.56	0.529	0.4657
Video-LLaVA-7B	Coarse	0.5318	0.5302	0.5269	0.5234	0.3369	0.3204	0.3032	0.2921
	Medium	0.5002	0.5	0.5006	0.5	0.2599	0.2563	0.2539	0.2521
	Mixed	0.5016	0.5018	0.5013	0.5005	0.2549	0.2544	0.2535	0.2519
	Fine	0.5	0.5	0.5001	0.5	0.2533	0.2531	0.2519	0.2514
LongVILA-8B	Coarse	0.853	0.8501	0.8398	0.8055	0.8575	0.8374	0.8026	0.7547
	Medium	0.7622	0.7422	0.7071	0.6768	0.6065	0.5771	0.5271	0.5007
	Mixed	0.6736	0.6489	0.6236	0.5998	0.4683	0.4417	0.4123	0.3945
	Fine	0.6898	0.6678	0.63	0.5764	0.4203	0.3956	0.3685	0.3332
LLaMA-VID-7B	Coarse	0.549	0.5387	0.5295	0.525	0.3751	0.3422	0.3151	0.2932
	Medium	0.5074	0.5038	0.5024	0.5003	0.2608	0.2534	0.2503	0.2482
	Mixed	0.5075	0.5054	0.5005	0.5001	0.2606	0.2549	0.2527	0.2502
	Fine	0.502	0.5002	0.4993	0.4994	0.2693	0.26	0.2548	0.252
InternVL2.5-78B	Coarse	0.9339	0.9264	0.9231	0.9025	0.9537	0.9453	0.9402	0.931
	Medium	0.8926	0.8884	0.8793	0.8521	0.8973	0.8872	0.8636	0.8258
	Mixed	0.7603	0.7322	0.7289	0.7165	0.7618	0.7407	0.7138	0.6877
	Fine	0.814	0.7967	0.7711	0.762	0.7811	0.7618	0.7483	0.6995
VideoXL-7B	Coarse	0.7957	0.7833	0.7574	0.7307	0.8142	0.7908	0.7629	0.7051
	Medium	0.645	0.6193	0.5974	0.5692	0.5739	0.5336	0.4934	0.453
	Mixed	0.621	0.6025	0.5789	0.5574	0.4549	0.4256	0.4117	0.3726
	Fine	0.6142	0.5898	0.5623	0.5287	0.4205	0.3958	0.3673	0.3472
Qwen2-VL-72B	Coarse	0.8835	0.8926	0.8942	0.8868	0.9167	0.9108	0.8923	0.8956
	Medium	0.7901	0.7785	0.7521	0.7157	0.7879	0.7483	0.702	0.6498
	Mixed	0.7017	0.6893	0.6702	0.643	0.6423	0.6187	0.5909	0.5463
	Fine	0.7198	0.6818	0.6545	0.6273	0.6456	0.6145	0.5943	0.5589
Oryx-7B	Coarse	0.7402	0.7136	0.6882	0.6635	0.6948	0.6566	0.6106	0.5644
	Medium	0.6841	0.6614	0.6392	0.6185	0.5907	0.5559	0.5182	0.4808
	Mixed	0.6246	0.6099	0.5946	0.5823	0.4858	0.46	0.428	0.4073
	Fine	0.6261	0.6074	0.591	0.5729	0.43	0.4094	0.3883	0.3666
LLaVA-Video-72B	Coarse	0.9132	0.9058	0.8826	0.8653	0.9503	0.9428	0.9276	0.9074
	Medium	0.9	0.8868	0.8727	0.8512	0.8662	0.8519	0.8291	0.798
	Mixed	0.7884	0.7893	0.7645	0.7587	0.7189	0.7003	0.6667	0.6229
	Fine	0.8099	0.8041	0.7694	0.7463	0.6961	0.7003	0.6742	0.6136
Qwen2-VL-7B	Coarse	0.8926	0.8846	0.8733	0.8615	0.8667	0.7656	0.714	0.7225

Continued on next page

Model	Grain	Binary Task				Multi-Choice Task			
		Short	Medium	Long	Origin	Short	Medium	Long	Origin
	Medium	0.7458	0.6734	0.631	0.6316	0.7082	0.5684	0.4832	0.5047
	Mixed	0.7098	0.6504	0.6158	0.612	0.6117	0.5165	0.4432	0.4639
	Fine	0.7068	0.6235	0.5873	0.5895	0.5254	0.409	0.3565	0.3655
VILA1.5-8B	Coarse	0.9062	0.9026	0.88	0.8662	0.9088	0.8909	0.8429	0.8099
	Medium	0.665	0.6574	0.6268	0.6066	0.6344	0.5861	0.4827	0.4486
	Mixed	0.6205	0.6188	0.5969	0.5743	0.5039	0.4587	0.393	0.3654
	Fine	0.6097	0.5941	0.5625	0.542	0.4369	0.3918	0.3297	0.3082
Qwen2-VL-2B	Coarse	0.8965	0.8907	0.8733	0.844	0.8618	0.8346	0.8027	0.7753
	Medium	0.6468	0.619	0.5969	0.5691	0.5512	0.514	0.4787	0.4564
	Mixed	0.6437	0.6093	0.5908	0.5633	0.4428	0.4137	0.3914	0.374
	Fine	0.6292	0.595	0.573	0.5493	0.3908	0.3613	0.3465	0.3344
Oryx1.5-7B	Coarse	0.7492	0.7222	0.6925	0.6674	0.705	0.6676	0.6239	0.584
	Medium	0.6921	0.6663	0.6474	0.622	0.5724	0.5447	0.5068	0.4752
	Mixed	0.6359	0.6223	0.6044	0.5972	0.472	0.4519	0.4266	0.4027
	Fine	0.6417	0.6193	0.6004	0.5848	0.4438	0.4246	0.3969	0.3826
LLaMA-VID-13B	Coarse	0.7542	0.7471	0.6879	0.6212	0.5748	0.5167	0.4571	0.3938
	Medium	0.5942	0.5742	0.5553	0.5498	0.3218	0.2897	0.2557	0.2304
	Mixed	0.5765	0.5641	0.5427	0.531	0.2987	0.2741	0.2561	0.2419
	Fine	0.5606	0.5411	0.526	0.5143	0.2725	0.2628	0.2518	0.2395
LLaVA-OneVision-72B	Coarse	0.8347	0.8017	0.786	0.7793	0.8838	0.8577	0.8258	0.8215
	Medium	0.8107	0.8025	0.7727	0.7273	0.7778	0.7399	0.7222	0.6684
	Mixed	0.7421	0.7132	0.6917	0.6603	0.6347	0.6035	0.5901	0.537
	Fine	0.7876	0.757	0.7116	0.6678	0.6103	0.601	0.5741	0.5118
Oryx1.5-32B	Coarse	0.7493	0.7156	0.6939	0.6712	0.7029	0.6643	0.6226	0.5697
	Medium	0.6911	0.6605	0.6461	0.6138	0.5967	0.5601	0.5325	0.4801
	Mixed	0.6563	0.6405	0.6178	0.6037	0.4787	0.45	0.4295	0.4055
	Fine	0.6445	0.6209	0.6015	0.588	0.4341	0.3989	0.3975	0.3831
LLaMA-VID-Long-Video	Coarse	0.5014	0.5115	0.5117	0.5017	0.2746	0.2804	0.2715	0.2629
	Medium	0.5034	0.49	0.496	0.4894	0.2792	0.2844	0.2824	0.2637
	Mixed	0.5055	0.4957	0.5	0.4932	0.281	0.283	0.2765	0.2674
	Fine	0.5135	0.5055	0.508	0.5051	0.2892	0.2932	0.2859	0.2754
LLaVA-NeXT-Video-7B	Coarse	0.8133	0.7972	-	0.7293	0.7287	0.6973	-	0.5788
	Medium	0.6353	0.6148	-	0.5717	0.482	0.4491	-	0.367
	Mixed	0.6102	0.5951	-	0.5547	0.4005	0.3775	-	0.3148
	Fine	0.6082	0.5871	-	0.5351	0.3634	0.3408	-	0.2941
LLaVA-OneVision-7B-chat	Coarse	0.916	0.9103	0.9021	0.8823	0.9035	0.8858	0.8793	0.8408
	Medium	0.8165	0.7852	0.7614	0.711	0.7301	0.6944	0.6753	0.6023
	Mixed	0.7375	0.7093	0.688	0.6547	0.618	0.5854	0.5641	0.5066
	Fine	0.7173	0.6835	0.6582	0.6205	0.5084	0.495	0.4745	0.4158
LLaVA-OneVision-7B	Coarse	0.9148	0.9084	0.902	0.8802	0.9015	0.8816	0.8758	0.8365
	Medium	0.817	0.7867	0.7624	0.7107	0.7276	0.6904	0.6742	0.6011
	Mixed	0.7377	0.7104	0.6883	0.6543	0.6164	0.5815	0.5638	0.5051
	Fine	0.7183	0.6833	0.6615	0.6204	0.5077	0.4928	0.4738	0.4135
InternVL2.5-8B	Coarse	0.8361	0.8424	0.8389	0.8201	0.9042	0.9079	0.9006	0.8834
	Medium	0.7086	0.7156	0.7064	0.6774	0.7628	0.7617	0.7519	0.7165
	Mixed	0.6635	0.6559	0.6522	0.623	0.6097	0.5995	0.5844	0.545
	Fine	0.6589	0.6564	0.6356	0.6049	0.5461	0.5339	0.5181	0.4808
VideoLLaMA2.1-7B	Coarse	0.6888	0.7307	0.7339	0.6967	0.8368	0.8215	0.8011	0.7347
	Medium	0.5982	0.5911	0.5839	0.5655	0.5322	0.4913	0.4599	0.4216
	Mixed	0.5702	0.5649	0.5573	0.5408	0.4629	0.4301	0.4079	0.3768
	Fine	0.5557	0.5488	0.5357	0.5222	0.3602	0.3443	0.3281	0.3082
Continued on next page									

Model	Grain	Binary Task				Multi-Choice Task			
		Short	Medium	Long	Origin	Short	Medium	Long	Origin
LLaVA-NeXT-Video-32B	Coarse	0.8238	0.8052	0.7735	0.7438	0.9147	0.8961	0.8758	0.8552
	Medium	0.665	0.6492	0.6335	0.5917	0.5855	0.5686	0.5353	0.4798
	Mixed	0.6105	0.6015	0.5818	0.5802	0.4787	0.4545	0.43	0.3712
	Fine	0.57	0.5663	0.5453	0.5471	0.4231	0.4017	0.3749	0.3401
Aria	Coarse	0.9081	0.9148	0.9101	0.8991	0.8335	0.8119	0.7953	0.7736
	Medium	0.7431	0.7386	0.7083	0.6934	0.7434	0.7116	0.679	0.655
	Mixed	0.7015	0.6897	0.6636	0.6445	0.5803	0.5187	0.4985	0.4818
	Fine	0.6802	0.6695	0.6346	0.615	0.5537	0.5082	0.4789	0.447

Table 20: JS Divergence performances on Character Hallucination

Model	Grain	Binary Task				Multi-Choice Task			
		Short	Medium	Long	Origin	Short	Medium	Long	Origin
Aria	Coarse	0.0014	0.0007	0.0008	0.0006	0.0006	0.001	0.0011	0.001
	Medium	0.0229	0.0197	0.0261	0.0292	0.003	0.0026	0.0042	0.0066
	Mixed	0.0263	0.0232	0.0274	0.0297	0.0009	0.0019	0.0023	0.0028
	Fine	0.0275	0.0207	0.0263	0.0314	0.0023	0.0044	0.0037	0.006
InternVL2.5-78B	Coarse	0.0009	0.0006	0.0007	0.001	0.0001	0.0001	0.0002	0.0003
	Medium	0.0017	0.0028	0.0036	0.0041	0.0003	0.0003	0.0006	0.0009
	Mixed	0.0144	0.0175	0.0185	0.0191	0.0011	0.0013	0.0033	0.0033
	Fine	0.0035	0.0045	0.0051	0.0045	0.0044	0.0046	0.0047	0.0064
InternVL2.5-8B	Coarse	0.0007	0.0009	0.001	0.0014	0.0005	0.0003	0.0002	0.0003
	Medium	0.0001	0.0002	0.0004	0.001	0.0032	0.0026	0.0025	0.0029
	Mixed	0.0003	0.0002	0.0	0.0001	0.0047	0.004	0.0036	0.0039
	Fine	0.0001	0.0003	0.001	0.0027	0.0115	0.0131	0.0119	0.0146
LLaMA-VID-13B	Coarse	0.0005	0.0023	0.0333	0.0743	0.0166	0.0331	0.0605	0.0902
	Medium	0.0094	0.0027	0.0008	0.0211	0.006	0.0157	0.0259	0.0344
	Mixed	0.002	0.0	0.0053	0.0315	0.0011	0.009	0.0224	0.0331
	Fine	0.0003	0.0024	0.0139	0.0439	0.0252	0.0469	0.0641	0.0809
LLaMA-VID-7B	Coarse	0.117	0.1279	0.1376	0.1483	0.193	0.2366	0.2819	0.3386
	Medium	0.164	0.1843	0.1939	0.2059	0.2474	0.3	0.3912	0.4563
	Mixed	0.0894	0.1073	0.1249	0.1479	0.3001	0.3386	0.3969	0.4408
	Fine	0.1798	0.1918	0.2059	0.2103	0.3434	0.4142	0.487	0.5172
LLaMA-VID-Long-Video	Coarse	0.0414	0.0347	0.0181	0.0291	0.284	0.2742	0.2848	0.3193
	Medium	0.035	0.0176	0.0088	0.0089	0.266	0.2454	0.245	0.2621
	Mixed	0.0193	0.0148	0.0082	0.0108	0.2418	0.2303	0.2275	0.247
	Fine	0.0283	0.025	0.0211	0.0155	0.2741	0.2586	0.265	0.2642
LLaVA-NeXT-Video-32B	Coarse	0.0133	0.0177	0.0241	0.0309	0.0003	0.0002	0.0006	0.0015
	Medium	0.0002	0.0004	0.0009	0.0042	0.0032	0.0044	0.0041	0.0067
	Mixed	0.0005	0.0039	0.0054	0.0119	0.0022	0.0044	0.0061	0.01
	Fine	0.0001	0.0001	0.0002	0.0003	0.0006	0.0027	0.0039	0.0102
LLaVA-Video-7B	Coarse	0.0004	0.0008	0.0015	0.0031	0.0001	0.0001	0.0001	0.0001
	Medium	0.0009	0.0005	0.0003	0.0001	0.001	0.0013	0.0012	0.0014
	Mixed	0.0008	0.0002	0.0	0.0001	0.0015	0.0015	0.0011	0.0007
	Fine	0.0012	0.0006	0.0002	0.0	0.006	0.0045	0.0031	0.0022
LLaVA-NeXT-Video-7B	Coarse	0.0082	0.0093	-	0.024	0.0173	0.0234	-	0.0554
	Medium	0.0357	0.0366	-	0.0417	0.0108	0.0146	-	0.0266
	Mixed	0.0394	0.0373	-	0.0462	0.018	0.0232	-	0.0357
	Fine	0.0218	0.0215	-	0.0238	0.0318	0.038	-	0.0435
LLaVA-OneVision-0.5B	Coarse	0.2158	0.2158	0.2158	0.2158	0.0119	0.013	0.0132	0.0101

Continued on next page

Model	Grain	Binary Task				Multi-Choice Task			
		Short	Medium	Long	Origin	Short	Medium	Long	Origin
	Medium	0.2158	0.2158	0.2158	0.2157	0.0154	0.0229	0.0227	0.0139
	Mixed	0.2158	0.2158	0.2158	0.2155	0.0218	0.0325	0.0299	0.0202
	Fine	0.2158	0.2158	0.2158	0.2157	0.0201	0.0374	0.047	0.0444
LLaVA-OneVision-72B	Coarse	0.0119	0.0166	0.0194	0.0208	0.0008	0.0008	0.0013	0.0011
	Medium	0.0143	0.0149	0.0205	0.0313	0.0008	0.0016	0.0019	0.0016
	Mixed	0.0099	0.0079	0.0146	0.0201	0.0007	0.0006	0.0012	0.0012
	Fine	0.003	0.0032	0.0081	0.0124	0.0009	0.0015	0.0042	0.0041
LLaVA-OneVision-7B	Coarse	0.0005	0.0005	0.0007	0.0006	0.0012	0.0024	0.0029	0.0041
	Medium	0.0006	0.0014	0.0017	0.0042	0.0035	0.006	0.0051	0.0079
	Mixed	0.0023	0.005	0.0055	0.0096	0.0079	0.0112	0.0098	0.0134
	Fine	0.0024	0.0054	0.0069	0.0126	0.0117	0.0102	0.0063	0.007
LLaVA-OneVision-7B-chat	Coarse	0.0004	0.0005	0.0008	0.0008	0.0011	0.0021	0.0025	0.0035
	Medium	0.0006	0.0014	0.0016	0.0039	0.0034	0.0052	0.0044	0.0065
	Mixed	0.0022	0.005	0.0052	0.0089	0.0078	0.01	0.0082	0.011
	Fine	0.0025	0.0058	0.007	0.0125	0.0103	0.0078	0.0045	0.005
LLaVA-Video-72B	Coarse	0.0006	0.0018	0.0036	0.0042	0.0001	0.0	0.0001	0.0002
	Medium	0.0	0.0003	0.0015	0.0013	0.0003	0.0006	0.0003	0.0008
	Mixed	0.0001	0.0	0.0001	0.0002	0.0006	0.001	0.0003	0.001
	Fine	0.0002	0.0	0.0001	0.0002	0.0028	0.0011	0.0039	0.0054
LongVILA-8B	Coarse	0.0046	0.0052	0.0071	0.0139	0.0093	0.0121	0.0188	0.0301
	Medium	0.0017	0.0011	0.0007	0.0021	0.0534	0.0545	0.0641	0.0684
	Mixed	0.0146	0.0126	0.0112	0.0175	0.0697	0.0688	0.0783	0.0822
	Fine	0.0086	0.0068	0.0052	0.0122	0.0984	0.0866	0.0871	0.0832
Oryx-7B	Coarse	0.0227	0.0301	0.0378	0.0469	0.0015	0.0016	0.0018	0.0014
	Medium	0.0383	0.0468	0.0553	0.0643	0.0038	0.0035	0.0041	0.004
	Mixed	0.0521	0.0588	0.0663	0.0749	0.0066	0.0064	0.0061	0.0059
	Fine	0.0441	0.0524	0.0616	0.0705	0.0253	0.0282	0.032	0.0358
Oryx1.5-32B	Coarse	0.025	0.0322	0.0381	0.0482	0.006	0.0069	0.0105	0.0125
	Medium	0.0276	0.035	0.0429	0.0478	0.0096	0.014	0.016	0.0198
	Mixed	0.036	0.0417	0.0457	0.0518	0.0197	0.0229	0.0275	0.0297
	Fine	0.0271	0.039	0.0443	0.0488	0.0136	0.0188	0.0201	0.0219
Oryx1.5-7B	Coarse	0.018	0.0231	0.0303	0.0356	0.002	0.0024	0.0035	0.0055
	Medium	0.0293	0.0376	0.0442	0.0503	0.0071	0.0085	0.0109	0.0121
	Mixed	0.0358	0.0436	0.0499	0.0547	0.0117	0.0133	0.0138	0.016
	Fine	0.0336	0.0417	0.0491	0.0563	0.0063	0.009	0.0127	0.0156
Qwen2-VL-2B	Coarse	0.0011	0.0012	0.0028	0.0058	0.0041	0.0069	0.0111	0.0136
	Medium	0.0379	0.0504	0.0622	0.0846	0.0587	0.0752	0.0918	0.1021
	Mixed	0.0245	0.0384	0.0516	0.0757	0.0705	0.0933	0.111	0.1121
	Fine	0.0249	0.0371	0.0477	0.0694	0.0868	0.1257	0.1482	0.154
Qwen2-VL-72B	Coarse	0.003	0.0027	0.0017	0.0019	0.0011	0.0013	0.0024	0.002
	Medium	0.015	0.0172	0.0221	0.0265	0.0067	0.0086	0.0145	0.0142
	Mixed	0.0271	0.0304	0.0316	0.042	0.0257	0.0272	0.038	0.0465
	Fine	0.0198	0.0267	0.0286	0.0364	0.019	0.0245	0.0265	0.0288
Qwen2-VL-7B	Coarse	0.0015	0.0009	0.0012	0.002	0.0001	0.0047	0.0053	0.0008
	Medium	0.0154	0.0217	0.0253	0.0237	0.0027	0.0043	0.032	0.0052
	Mixed	0.0109	0.0137	0.0171	0.0163	0.0059	0.0094	0.0593	0.0124
	Fine	0.009	0.014	0.0164	0.0151	0.0103	0.0631	0.0749	0.0236
VILA1.5-8B	Coarse	0.0016	0.0009	0.0006	0.0006	0.0006	0.0007	0.0013	0.0015
	Medium	0.0449	0.0371	0.0334	0.0349	0.0068	0.007	0.0097	0.0089
	Mixed	0.0578	0.0449	0.0325	0.0335	0.007	0.0074	0.0097	0.0086
	Fine	0.0609	0.0519	0.041	0.0387	0.0336	0.039	0.0531	0.049
Continued on next page									

Model	Grain	Binary Task				Multi-Choice Task			
		Short	Medium	Long	Origin	Short	Medium	Long	Origin
Video-LLaVA-7B	Coarse	0.1556	0.1536	0.1462	0.1448	0.344	0.3589	0.3755	0.387
	Medium	0.2115	0.2117	0.2117	0.2115	0.4697	0.4691	0.4781	0.4823
	Mixed	0.2048	0.2018	0.2007	0.2011	0.482	0.4811	0.4843	0.4868
	Fine	0.215	0.2153	0.215	0.2144	0.5126	0.512	0.5149	0.5137
VideoLLaMA2.1-7B	Coarse	0.0532	0.0365	0.0338	0.0456	0.0058	0.0039	0.0042	0.0048
	Medium	0.0582	0.0544	0.0506	0.0597	0.0054	0.0058	0.0044	0.0074
	Mixed	0.0745	0.0705	0.0659	0.0745	0.0094	0.0096	0.0096	0.011
	Fine	0.0647	0.0662	0.0615	0.0657	0.0195	0.0104	0.0092	0.0121
VideoXL-7B	Coarse	0.0003	0.0003	0.0006	0.0007	0.0001	0.0002	0.0001	0.0001
	Medium	0.0052	0.0073	0.0092	0.0099	0.0053	0.0052	0.0056	0.0062
	Mixed	0.0038	0.0053	0.0081	0.0095	0.009	0.0097	0.0085	0.01
	Fine	0.0037	0.0055	0.0089	0.01	0.0076	0.0085	0.0112	0.0151

Table 21: LVMs’ on Stage: Non-dialogue for Binary tasks

LVM	W Avg	JSD	EA	COV	AOV	SA	MIV
GPT-4o	.81407	.00033	.72115	.94059	.93069	.89000	.86667
Gemini1.5-Pro	.73256	.00007	.57843	.95050	.87129	.85000	.87500
Claude 3.5-Sonnet	.72956	.00059	.53846	.99010	.91089	.89000	.89167
InternVL2.5-78B	.85254	.00005	.77170	.97843	.95092	.92500	.87917
LLaVA-Video-72B	.83019	.00936	.87942	.87211	.80675	.79500	.65000
LLaVA-Video-7B	.80974	.00803	.85490	.89104	.85394	.78000	.53333
LLaVA-OneVision-7B-chat	.78596	.01446	.87982	.89398	.77693	.69750	.40000
LLaVA-OneVision-7B	.78495	.01481	.87982	.89020	.77677	.69333	.40000
LLaVA-NeXT-Video-32B	.78447	.01730	.86174	.74632	.75997	.72250	.60000
Qwen2VL-7B	.78279	.00991	.80868	.89861	.79564	.77083	.56250
LLaVA-OneVision-72B	.77736	.03623	.94695	.73721	.63574	.60819	.45000
Aria-23B	.77530	.00026	.67042	.94629	.91777	.89000	.76667
Qwen2VL-72B	.74846	.00415	.55064	.98108	.96319	.94083	.90000
VILA1.5-8B	.73806	.02415	.82195	.82064	.71019	.69833	.38750
InternVL2.5-8B	.71039	.05260	.85002	.65049	.64297	.61829	.37131
Qwen2VL-2B	.69379	.00119	.47548	.97378	.93541	.93083	.80833
VideoXL-7B	.66517	.00787	.54976	.80415	.82631	.79732	.69456
VideoLLaMA2.1-7B	.65353	.00311	.38505	.96340	.95627	.95583	.81250
LongVILA-8B	.64279	.12937	.94534	.55168	.33016	.32500	.15417
LLaMA-VID-13B	.62602	.02439	.59188	.73056	.71923	.66165	.52917
Oryx1.5-7B	.59861	.00414	.26125	.95597	.93710	.92583	.92500
Oryx-7B	.59579	.00650	.24397	.97125	.94584	.93167	.94167
Oryx1.5-32B	.59453	.00669	.24598	.97588	.94477	.93083	.92083
LLaVA-NeXT-Video-7B	.58980	.01182	.21584	.97840	.97330	.97000	.93333
LLaMA-VID-Long-Video-7B	.52466	.16089	.74719	.32913	.33691	.30083	.24167
LLaMA-VID-7B	.51225	.39224	.97588	.03225	.06722	.04917	.04583
Video-LLaVA-7B	.50402	.43679	.99116	.01641	.02363	.01500	.01250
VideoAgent	.58139	.00056	.33548	.81202	.84462	.87477	.77778
LLaVA-OneVision-0.5B	.50056	.46938	.99799	.00224	.00445	.00167	.00417

Table 22: LVMs’ on Stage: Non-dialogue for Multi-choice tasks

LVM	Metrics	Overall	COV	AOV	SA	MIV
GPT-4o	Accuracy	.67338	.63492	.80620	.80952	.44286
	OB	.02344	.04940	.01586	.02280	.03945
	COB	.01663	.05796	.03189	.02246	.02908
	JSD	.00251	.00262	.00308	.00060	.01370
Gemini1.5-Pro	Accuracy	.60624	.63492	.65116	.67460	.46429
	OB	.02104	.04811	.07134	.04143	.01956
	COB	.02612	.05728	.07576	.04353	.01276
	JSD	.00084	.00477	.00434	.00353	.00974
Claude 3.5-Sonnet	Accuracy	.75106	.80952	.82171	.73016	.64286
	OB	.03370	.05219	.05409	.04105	.07053
	COB	.02812	.04926	.05399	.03994	.06111
	JSD	.00197	.00166	.00420	.00478	.00692
InternVL2.5-78B	Accuracy	.85534	.90517	.90575	.86399	.74643
	OB	.01309	.02149	.01321	.01352	.03847
	COB	.00989	.01996	.01138	.01234	.04037

Continued on next page...

LVM	Metrics	Overall	COV	AOV	SA	MIV
	JSD	.00017	.00037	.00017	.00007	.00070
LLaVA-Video-72B	Accuracy	.82966	.87759	.90575	.84602	.68929
	OB	.01253	.01764	.01202	.02064	.01451
	COB	.01049	.01877	.00995	.01544	.03305
	JSD	.00014	.00009	.00017	.00042	.00078
LLaVA-Video-7B	Accuracy	.82264	.90597	.89769	.83690	.65000
	OB	.01107	.00856	.01483	.01348	.04315
	COB	.00716	.00674	.01092	.00946	.04891
	JSD	.00013	.00002	.00015	.00036	.00077
InternVL2.5-8B	Accuracy	.76609	.86451	.83795	.77707	.58484
	OB	.01530	.01752	.01912	.01089	.00469
	COB	.00924	.01388	.01276	.00437	.02411
	JSD	.00042	.00031	.00063	.00041	.00119
LLaVA-NeXT-Video-32B	Accuracy	.76125	.80259	.86155	.78443	.59643
	OB	.01691	.02196	.01900	.01792	.07012
	COB	.01277	.01811	.01520	.01490	.06845
	JSD	.00029	.00021	.00037	.00051	.00456
LLaVA-OneVision-7B-chat	Accuracy	.74606	.84214	.84042	.79812	.50357
	OB	.02528	.02247	.02685	.02972	.02661
	COB	.01474	.02012	.01434	.01159	.03452
	JSD	.00150	.00083	.00175	.00220	.00584
LLaVA-OneVision-7B	Accuracy	.74177	.83696	.83570	.79441	.50000
	OB	.02940	.02717	.02996	.03354	.03369
	COB	.01701	.02265	.01534	.01396	.03388
	JSD	.00198	.00129	.00215	.00273	.00695
Qwen2VL-72B	Accuracy	.73912	.78190	.79066	.81608	.56786
	OB	.04514	.04403	.04860	.03183	.10561
	COB	.02893	.02652	.03271	.02212	.10462
	JSD	.00467	.00569	.00536	.00218	.01697
LLaVA-OneVision-72B	Accuracy	.73003	.78362	.77731	.76989	.58929
	OB	.02153	.02809	.01909	.02765	.02513
	COB	.01364	.02409	.01235	.01505	.03866
	JSD	.00055	.00055	.00048	.00125	.00141
VILA1.5-8b	Accuracy	.69174	.79685	.77287	.72940	.46786
	OB	.02914	.03352	.03052	.02456	.03562
	COB	.01625	.02140	.01727	.01065	.02665
	JSD	.00180	.00169	.00198	.00179	.00425
Aria-23B	Accuracy	.67730	.68989	.71031	.78757	.52143
	OB	.02706	.03333	.02448	.02604	.02461
	COB	.01794	.02994	.01665	.00998	.03407
	JSD	.00152	.00198	.00098	.00174	.00144
Qwen2VL-7B	Accuracy	.67171	.71857	.72894	.76076	.47857
	OB	.06840	.07078	.07165	.05800	.15205
	COB	.04717	.04231	.05362	.04366	.13459
	JSD	.01047	.01187	.01151	.00747	.04513
Qwen2VL-2B	Accuracy	.64973	.65862	.74368	.76447	.43214
	OB	.07865	.09046	.07532	.06471	.11172
	COB	.05239	.06150	.05166	.04195	.10970

Continued on next page...

LVM	Metrics	Overall	COV	AOV	SA	MIV
	JSD	.01380	.01866	.01263	.00935	.02842
VideoLLaMA2.1-7B	Accuracy	.63791	.65236	.75480	.75877	.38571
	OB	.05798	.07124	.04685	.04163	.19722
	COB	.02626	.02505	.02445	.02510	.16654
	JSD	.00588	.01021	.00357	.00253	.04725
LongVILA-8B	Accuracy	.60895	.65797	.66083	.64557	.47143
	OB	.11411	.12307	.10548	.11037	.12748
	COB	.08391	.09547	.07543	.07740	.08819
	JSD	.03425	.03846	.02975	.03262	.05534
VideoXL-7B	Accuracy	.59611	.63060	.69331	.63964	.42086
	OB	.04204	.03565	.04169	.04851	.08392
	COB	.02596	.01550	.02870	.03487	.08361
	JSD	.00335	.00288	.00303	.00460	.00752
LLaVA-NeXT-Video-7B	Accuracy	.55734	.51736	.66741	.64461	.40000
	OB	.06321	.08413	.04757	.05487	.03360
	COB	.03847	.06915	.02555	.02145	.01786
	JSD	.00891	.01429	.00546	.00721	.00823
LLaVA-OneVision-0.5B	Accuracy	.49069	.48135	.57492	.54577	.36071
	OB	.11133	.12498	.09776	.10805	.11359
	COB	.07676	.09557	.06184	.07369	.08699
	JSD	.02462	.03015	.01918	.02433	.02648
Oryx1.5-32B	Accuracy	.47065	.51758	.49124	.54520	.32857
	OB	.05783	.07413	.06159	.03452	.05107
	COB	.03068	.02995	.03955	.02555	.02306
	JSD	.00655	.01225	.00709	.00211	.00473
Oryx-7B	Accuracy	.46555	.50205	.50236	.52923	.32857
	OB	.03317	.04875	.02088	.02834	.06911
	COB	.01657	.02025	.00929	.02504	.06700
	JSD	.00230	.00585	.00124	.00122	.00784
Oryx1.5-7B	Accuracy	.48457	.55661	.50570	.52238	.35357
	OB	.05427	.06030	.05390	.04817	.06522
	COB	.03274	.02756	.03673	.03772	.05731
	JSD	.00601	.00826	.00612	.00432	.00512
VideoAgent	Accuracy	.40169	.37671	.38631	.46018	.38356
	OB	.04951	.05674	.05547	.03348	.07526
	COB	.05376	.08826	.05472	.02451	.03571
	JSD	.00409	.00288	.00500	.00568	.01923
LLaMA-VID-13B	Accuracy	.37579	.35728	.45010	.44223	.25357
	OB	.13043	.13447	.11696	.14326	.10824
	COB	.08911	.11056	.07094	.08812	.09148
	JSD	.03114	.03181	.02676	.03735	.02803
LLaMA-VID-7B	Accuracy	.34046	.31324	.40391	.40097	.24373
	OB	.27100	.30786	.24318	.24774	.30998
	COB	.19869	.26168	.16361	.16729	.26735
	JSD	.11762	.15328	.09503	.09741	.18199
Video-LLaVA-7B	Accuracy	.26384	.26957	.28135	.28657	.21786
	OB	.39500	.40049	.39634	.38562	.40438
	COB	.35356	.37054	.34716	.33635	.39555

Continued on next page...

LVM	Metrics	Overall	COV	AOV	SA	MIV
	JSD	.28011	.28973	.28253	.26252	.33570
LLaMA-VID-Long-Video-7B	Accuracy	.24726	.26634	.25910	.26718	.19643
	OB	.31721	.32747	.30794	.31516	.29721
	COB	.30468	.32098	.29409	.29500	.29016
	JSD	.19453	.20196	.19326	.18820	.18904

Table 23: LVMs’ on Stage: Dialogue for Multi-choice tasks

LVM	Metrics	Overall	COV	CIV
GPT-4o	Accuracy	.73359	.81853	.64865
	OB	.02294	.03816	.01647
	COB	.01870	.03285	.00729
	JSD	.00172	.00198	.00154
Gemini1.5-Pro	Accuracy	.77889	.83051	.72727
	OB	.02783	.03241	.02340
	COB	.02425	.03166	.01926
	JSD	.00126	.00134	.00165
Claude 3.5-Sonnet	Accuracy	.77799	.88417	.67181
	OB	.02711	.03425	.02274
	COB	.02263	.02919	.02207
	JSD	.00129	.00150	.00223
InternVL2.5-78B	Accuracy	.83820	.94886	.72755
	OB	.01543	.00988	.02209
	COB	.01114	.00711	.01686
	JSD	.00034	.00021	.00088
LLaVA-Video-72B	Accuracy	.82166	.92351	.71981
	OB	.00290	.00756	.00178
	COB	.00526	.00544	.00578
	JSD	.00014	.00036	.00005
LLaVA-Video-7B	Accuracy	.81951	.93124	.70778
	OB	.01033	.00685	.01401
	COB	.00862	.00643	.01270
	JSD	.00012	.00005	.00031
Qwen2VL-72B	Accuracy	.79387	.91147	.67627
	OB	.05425	.02754	.08116
	COB	.03737	.01953	.06146
	JSD	.00559	.00102	.01483
VILA1.5-8B	Accuracy	.78814	.89686	.67942
	OB	.01139	.00977	.01502
	COB	.00895	.00539	.01394
	JSD	.00029	.00033	.00053
LLaVA-OneVision-72B	Accuracy	.78513	.88354	.68672
	OB	.00672	.00478	.01380
	COB	.00722	.00529	.01158
	JSD	.00009	.00021	.00033
InternVL2.5-8B	Accuracy	.78061	.90102	.66020
	OB	.01118	.00854	.01494
	COB	.00644	.00319	.01147
Continued on next page...				

LVM	Metrics	Overall	COV	CIV
	JSD	.00044	.00031	.00078
LongVILA-8B	Accuracy	.76472	.85131	.67813
	OB	.05053	.04321	.05795
	COB	.02672	.02318	.03182
	JSD	.00679	.00544	.00840
Aria-23B	Accuracy	.75330	.85039	.65621
	OB	.01528	.01867	.02041
	COB	.00845	.01039	.01060
	JSD	.00081	.00132	.00110
LLaVA-NeXT-Video-32B	Accuracy	.75118	.85905	.64332
	OB	.01603	.02019	.01439
	COB	.00621	.00626	.00764
	JSD	.00059	.00117	.00034
LLaVA-OneVision-7B-chat	Accuracy	.75075	.89729	.60421
	OB	.01435	.00568	.02511
	COB	.00836	.00269	.01821
	JSD	.00059	.00035	.00130
LLaVA-OneVision-7B	Accuracy	.74839	.89514	.60163
	OB	.01405	.00533	.02478
	COB	.00847	.00340	.01768
	JSD	.00058	.00032	.00128
Qwen2VL-7B	Accuracy	.74710	.85131	.64289
	OB	.05738	.04220	.07338
	COB	.03913	.02779	.05467
	JSD	.00655	.00310	.01188
Oryx1.5-32B	Accuracy	.74602	.85303	.63902
	OB	.03544	.02817	.04350
	COB	.02362	.01633	.03381
	JSD	.00189	.00097	.00328
Oryx1.5-7B	Accuracy	.74431	.83455	.65406
	OB	.02129	.01773	.02691
	COB	.01510	.01329	.01779
	JSD	.00062	.00042	.00116
Oryx-7B	Accuracy	.74108	.83025	.65191
	OB	.02634	.02869	.02796
	COB	.01075	.00799	.01564
	JSD	.00139	.00212	.00123
VideoLLaMA2.1-7B	Accuracy	.74044	.83928	.64160
	OB	.02815	.01974	.03885
	COB	.01748	.01277	.02496
	JSD	.00112	.00037	.00260
Qwen2VL-2B	Accuracy	.72733	.83627	.61839
	OB	.06667	.05269	.08306
	COB	.04773	.03588	.06447
	JSD	.00996	.00569	.01687
LLaVA-OneVision-0.5B	Accuracy	.72174	.82639	.61710
	OB	.03995	.03636	.04382
	COB	.02286	.01849	.03009
Continued on next page...				

LVM	Metrics	Overall	COV	CIV
	JSD	.00454	.00401	.00511
VideoXL-7B	Accuracy	.71612	.81298	.61925
	OB	.01767	.01337	.02310
	COB	.01489	.01064	.02077
	JSD	.00034	.00013	.00075
LLaVA-NeXT-Video-7B	Accuracy	.65813	.73709	.57917
	OB	.07936	.08412	.07471
	COB	.03629	.03377	.03997
	JSD	.01391	.01591	.01207
LLaMA-VID-13B	Accuracy	.54598	.63086	.46111
	OB	.10499	.09757	.11302
	COB	.05561	.04498	.07061
	JSD	.02018	.01838	.02260
LLaMA-VID-7B	Accuracy	.36506	.39708	.33305
	OB	.30118	.29315	.30920
	COB	.21621	.19421	.24258
	JSD	.15487	.14768	.16252
LLaMA-VID-Long-Video-7B	Accuracy	.30705	.30855	.30554
	OB	.21638	.21046	.22231
	COB	.20458	.19543	.21388
	JSD	.11542	.11025	.12105
Video-LLaVA-7B	Accuracy	.28578	.29308	.27847
	OB	.40171	.39936	.40407
	COB	.34912	.33238	.36678
	JSD	.29504	.29185	.29855

Table 24: LVMs’ on Stage: Dialogue for Binary tasks

LVM	Weighted Average	JSD	ET	COV	AOV	CIV
GPT-4o	.79326	.00003	.69672	.98347	.91736	.76860
Gemini1.5-Pro	.82319	.00166	.78689	.99174	.87603	.71074
Claude 3.5-Sonnet	.78094	.00004	.68033	.00000	.92562	.71901
LLaVA-Video-72B	.80595	.00951	.88146	.91864	.85269	.42000
LLaVA-Video-7B	.80082	.00683	.83326	.94538	.86734	.49241
VILA1.5-8B	.79207	.01546	.87799	.90231	.80995	.40621
InternVL2.5-78B	.79024	.00001	.72167	.98595	.95397	.63655
Qwen2VL-7B	.78416	.00837	.79939	.94538	.80694	.55448
LLaVA-OneVision-7B-chat	.78519	.01581	.87712	.91978	.79384	.36621
LLaVA-OneVision-7B	.78369	.01671	.87842	.91652	.78551	.36483
LLaVA-OneVision-72B	.77140	.02492	.92271	.80621	.72025	.33379
Qwen2VL-2B	.76223	.00095	.68736	.97232	.91002	.62897
LLaVA-NeXT-Video-32B	.75449	.02242	.88971	.73151	.84632	.28000
LLaVA-NeXT-Video-7B	.74967	.00006	.61435	.94146	.95229	.76121
Oryx1.5-32B	.74696	.00015	.61224	.97528	.89391	.77586
Oryx-7B	.74578	.00037	.61876	.96507	.89125	.76207
Oryx1.5-7B	.73947	.00070	.61919	.95249	.89160	.73517
Qwen2VL-72B	.73510	.00350	.57794	.98595	.96530	.72552
Aria-23B	.73221	.00001	.60703	.97661	.94793	.64759
LLaMA-VID-13B	.71878	.02283	.78637	.74452	.88009	.32897
VideoXL-7B	.71121	.01506	.69952	.79165	.84194	.53509
VideoLLaMA2.1-7B-16f	.69792	.00107	.49023	.97795	.96440	.77448
InternVL2.5-8B	.69924	.02956	.74727	.80786	.67040	.47540
LongVILA-8B	.65889	.12075	.93096	.61590	.30252	.24207
LLaMA-VID-7B	.51728	.40015	.99739	.01273	.09529	.00345
LLaMA-VID-Long-Video-7B	.50609	.24305	.80808	.19050	.17906	.24276
LLaVA-OneVision-0.5B	.50061	.47166	.99957	.00104	.00390	.00000
Video-LLaVA-7B	.50400	.45490	1.	.00148	.02249	.00000

E Additional Case Study

Setting Hallucination

Q: Are there chairs in the video? A: There are chairs in the video

Q: Is laundry basket visible in the video? A: Laundry basket is not visible in the video

Q: What is the object that appears in the video?

Options:

A. Test tube is visible in the video. B. Pipette is visible in the video.

C. Sofa is visible in the video. D. Aisle runner is visible in the video.

Q: What is the object present in the video?

Options:

A. Laundry basket presents in the video. B. Welding mask presents in the video.

C. Table presents in the video. D. Spare tire presents in the video.

Stage Hallucination (Non-Dialogue)

Q: Does the video depict a man in a button-up shirt without glasses pouring wine? A: The video shows a man in a button-up shirt without glasses pouring wine. (EA)

Q: Does the video show a man wearing a jacket and glasses pouring wine? A: The video does not depict a man wearing a jacket and glasses pouring wine. (MIV)

Q: Does the video show a woman in a dress and glasses noticing pretzels in the bowl? A: The video does not depict a woman in a dress and glasses noticing pretzels in the bowl. (AOV)

Q: Does the video show a man in a red lab coat walking behind someone? A: The video does not depict a man in a red lab coat walking behind someone. (POV)

Q: What happened in the video?

Options:

A: A woman wearing a brown vest sat on the brown leather sofa.

B: A woman wearing a brown vest applies a garland to the tree.

C: A man wearing a button-up shirt and not wearing glasses was in the cafeteria.

D: A man wearing a button-up shirt and not wearing glasses shows a Chinese star to a man wearing a jacket and glasses (AOV)

Q: What happened in the video?

Options:

A: A woman wearing a brown vest sat on the brown leather sofa.

B: A man wearing a button-up shirt and not wearing glasses was slicing bread for breakfast.

C: A man wearing a button-up shirt and not wearing glasses was stirring soup for lunch.

D: A woman wearing a dress and glasses jumped over the fence. (SA)

Character Hallucination

Q: Does a woman wearing brown vest appear in the video? A: A woman wearing brown vest appears in the video. (Coarse)

Q: Who appears in the video?

Options:

A: A man wearing short-sleeved green polo shirt and wearing glasses.

B: A woman wearing short-sleeved t-shirt and not wearing glasses.

C: A woman wearing long-sleeved jacket and not wearing glasses.

D: A man wearing long-sleeved jacket and wearing glasses. (Medium)

Q: Does a woman wearing light long-sleeved dress and not wearing glasses appear in the video? A: A woman wearing light long-sleeved dress and not wearing glasses does not appear in the video. (Mixed)

Q: Does the video show a person wearing collared brown vest with no pocket and wearing glasses? A: The video shows a person wearing collared brown vest with no pocket and wearing glasses. (Mixed)

Q: Who appears in the video?

Options:

A: A woman wearing dark long-sleeved collared jacket with no pocket and wearing glasses.

B: A man wearing long-sleeved collarless jacket and wearing glasses.

C: A man wearing light long-sleeved collared jacket with pockets and wearing glasses.

D: A woman wearing light long-sleeved collarless jacket with pockets and not wearing glasses. (Fine)

Stage Hallucination (Dialogue)

Q: Does the video depict a woman conversing while wearing a brown vest? A: The video shows a woman conversing while wearing a brown vest. (00:38 – 00:46) (ET)

Q: Does the video depict a man with a jacket and glasses conversing? A: The video does not show a man with a jacket and glasses conversing. (00:38 – 00:46) (CIV)

Q: Which individual was the one who spoke in the video?

Options:

A: A man in a white vest was speaking in the video.

B: A woman in a black polo shirt was speaking in the video.

C: A woman in a brown vest was speaking in the video.

D: A woman in a pink lab coat was speaking in the video. (00:38 – 00:46) (AOV)

Figure 19: An example of one video and part of its corresponding hallucination questions.

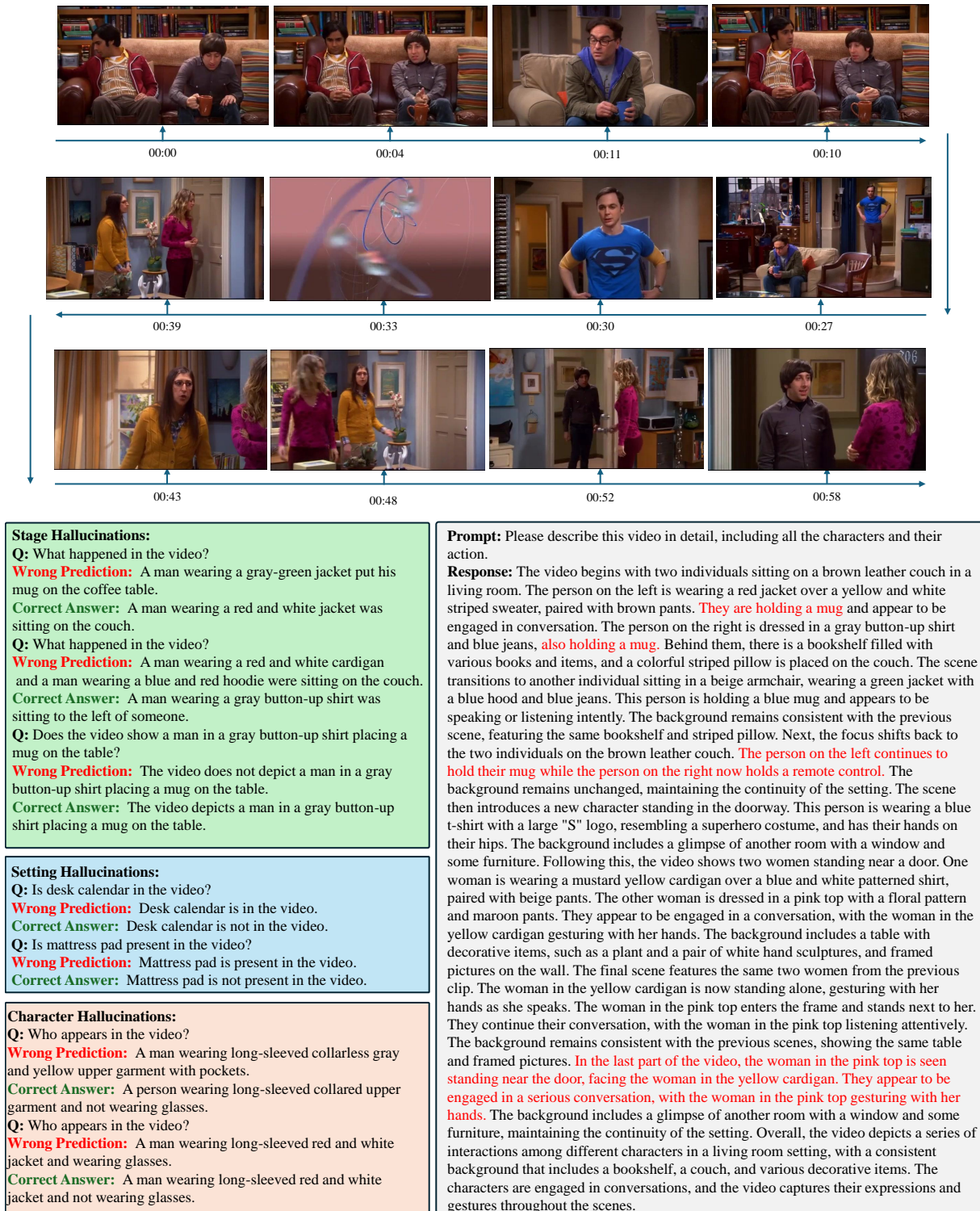


Figure 20: Analysis of video question answering and description tasks reveals that LVMs exhibit a tendency to avoid generating descriptions for content that elicits uncertainty, as specifically detected through question answering; instances of hallucinated content are highlighted in red.